이학석사 학위논문

Trapped Greenhouse Gas in Permafrost Active Layer

-Gas and Soil Properties of Frozen Alaskan Cores-

영구동토 활동층에 갇힌 온실기체

-얼어있는 알래스카 코어의 기체와 토양성분-

2016 년 2 월

서울대학교 대학원

지구환경과학부

변 은 지

Trapped Greenhouse Gas in Permafrost Active Layer

-Gas and Soil Properties of Frozen Alaskan Cores-

지도교수 안 진 호

이 논문을 이학석사 학위논문으로 제출함
2016년 2월

서울대학교 대학원
지구환경과학부
변 은 지

변은지의 이학석사 학위논문을 인준함
2015년 12월

위 원 장 _____ (인)

부위원장 _____ (인)

위 원 _____ (인)

Abstract

Trapped Greenhouse Gas in Permafrost Active Layer

Eunji Byun
School of Earth and Environmental Sciences
The Graduate School
Seoul National University

Permafrost at high northern latitudes is thought to contain a substantial amount of organic carbon that has accumulated since the last glacial period. Under warming conditions, greenhouse gas (GHG) emission to the atmosphere will inevitably occur through the decomposition of the stored carbon especially in near-surface permafrost. However, significant uncertainties still remain in incorporating this phenomenon into global carbon cycle models due to lack of robust estimation of the GHG emission. If the GHG efflux is merely extrapolated from surface measurements for a short period, the amount of GHG might be under- or overestimated. Previous studies suggested that a gas impermeable surface present during winter can temporarily hinder the emission of GHG formed at the subsurface. Such accumulated GHG can generate anomalously high efflux when it is outgassed all at once by seasonal thaw of the surface active layer. Nevertheless, previous research has relied on observation at the surface without sufficient consideration of the subsurface process. This study hypothesized that gas concentration profiles of winter soil columns would show a transition

state of subsurface trapped gas before spring release. To confirm this, five 90 cm-long soil cores were drilled at various latitudes and vegetation sites in Alaska during early spring of 2013, when the ground was still frozen and snow-covered. Vertical profiles of CO_2, CH_4, and other soil properties were analyzed within 5–10-cm depth resolutions. Interestingly, two CH_4 profiles revealed high concentrations (up to 416 $\mu mol_{CH4}\ L^{-1}{}_{soil}$) at certain depths implying frustrated GHG transport to the surface, named "CH_4 peaks". Temperature inversion in late autumn may promote the formation of such CH_4 peaks. That is, relatively warm underground conditions encourage microbial activity and the upper frozen layer inhibits upward transport of produced CH_4. The trapped CH_4 at shallow depths can be either released to the atmosphere or oxidized within soil columns as the temperature rise defrosts the surrounding matrix. In contrast, the CH_4 peak in the deeper layer might be preserved for several years depending on the maximum thaw depth (active layer thickness) in the coming years. Taking these findings into consideration, estimation of GHG efflux from permafrost soil columns can be complicated by the existence of trapped CH_4.

Key words : Permafrost, Greenhouse gas emission, Active layer, Methane, Gas permeability

Student Number : 2014-20325

Table of Contents

List of Tables

List of Figures

1. Introduction

1.1. Permafrost and greenhouse gas

1.1.1. Permafrost carbon feedback (PCF)

After the last glacial period (since ~12,000 years ago), regionally cold temperatures on Earth have maintained the frozen ground at North America, Siberia, Greenland, Antarctica and even some high mountains at low latitudes. Permafrost is defined as the perennially cryotic area that remains under 0°C for more than two consecutive years (French, 2007). This criterion is not applicable to continental ice sheets but to soils, rocks, ground ice and organic layers. Low temperature must have acted as a dominant soil forming factor on regionally unglaciated terrains at high latitudes during glacial periods. The exposed ground had been covered by wind-driven deposits (periglacial loess) or peat layers in some regions where precipitation and temperature conditions were suitable for seasonal plant growth (French, 2007). Then, repetitive freeze-thaw along with climate cycles made distinctive ground features such as permafrost polygons, sorted circles, and underground ice wedges. In addition, the ground contains relatively large amounts of partially- or un- decomposed organic matter because the cold temperature suppressed soil microbial activities.

Soil layers where permafrost occurs can be divided vertically into two parts the upper active layer and the lower permafrost. The active layer is only seasonally frozen, while the permafrost is perennially frozen (Fig. 1). Most permafrost has an active layer at surface with a thickness decided by the maximum thaw depth in a year. The existence of the active layer can be helpful to wipe out sudden atmospheric temperature changes and prevent a summer thaw of the permafrost below. Therefore, organic matters stored in the permafrost remain stable for more than a year, while those deposited in active

layers are relatively well decomposed by activated soil microbes during the growing season.

Although the most decisive factor is regional temperature, permafrost state and distribution is influenced by other environmental factors as well. Even under the same range of air temperature, ground thermal gradients can vary from place to place. For example, vegetation cover and topography creates heterogeneities of surface heat absorption and the penetration rate. As a result, where atmospheric temperature is not sufficiently low to freeze all of the surroundings, permafrost can be patchily distributed. Accordingly, permafrost is categorized by the existence of a horizontal area as continuous (>90%), discontinuous (50–90%), sporadic (10–50%), and isolated (<10%), roughly coinciding with latitudinal temperature changes (French, 2007). Permafrost thickness also varies locally from several to hundreds of meters. Generally, the sporadic or discontinuous permafrost is shallow and appears in lower latitudes compared to the thick continuous permafrost near the polar region.

It has been reported that temperature and active layer thickness have increased in almost all permafrost areas over the last 30 years (IPCC, 2013). Consequently, the original continuous permafrost is now becoming discontinuous or sporadic and more susceptible to thaw. This is problematic to local residents due to the more vulnerable surface for construction and maintenance of infrastructures (Osterkamp, 2003). Apart from such physical damage, another serious concern in the global context is expansion of the atmospheric carbon source in the global carbon cycle and its reinforcing impact on global warming (Schuur *et al.*, 2015; 2008; IPCC, 2013). The top active layer in most permafrost regions reaches only 0.3–1.5 m from the surface in the current climate condition, while the permafrost below rarely participates in annual carbon cycling. Thus, the expansion of active layer into deep permafrost

may result in an increase in the decomposable component and a decrease in the stable component of these terrestrial-carbon reservoirs.

The permafrost carbon pool in northern high latitudes is estimated to contain 1672 PgC which is twice as large as the atmospheric carbon pool (Schuur *et al.*, 2008; Tarnocai *et al.*, 2009). Once released to the atmosphere, it may take considerable time for the carbon to be re-captured by permafrost vegetation. In this regard, the decomposition of permafrost carbon can be considered as an irreversible component for millennia, comparable to the anthropogenic use of fossil fuels (Schaefer *et al.*, 2011). Specifically, more than 60 percent of the estimated carbon in the Arctic permafrost field (~1035 PgC) is residing in the surface 0–3 m layer, which is vulnerable to thaw by only a small rise of atmospheric temperature in decadal to centennial time scales (Schuur *et al.*, 2015). This shallow carbon will be injected to the atmosphere through the enlarged surface active layer within a few centuries so that it will boost the first part of permafrost carbon feedback (PCF). After that, the deeper reservoir may also take part in that positive feedback loop releasing its stored carbon as additional CO_2 and CH_4 to the atmosphere (more than or equal to millennia). It is therefore necessary to counter the PCF in the global carbon cycle in the context of recent climate warming and future climate projections (Anisimov, 2007; Schaefer *et al.*, 2014).

1.1.2 Greenhouse gas emission from permafrost

To measure the GHG efflux from permafrost soils, various methods have been used both in the field and in the laboratory. For example, chambers are installed at the soil surface to gather the released gas. The concentration of targeted GHG in the collected soil air is determined by portable gas analyzers (Friborg *et al.*, 1997; Heyer *et al.*, 2002; Kim *et al.*, 2014; 2013; 2007;

Mastepanov *et al.*, 2008; Sabrekov *et al.*, 2014; Song *et al.*, 2012; Yu *et al.*, 2007; Zimov *et al.*, 1996). An eddy covariance tower is also installed with a gas analyzer at 2–3 m from the soil surface to indirectly measure the GHG efflux by calculating cumulative changes in GHG concentration in the surrounding air (Friborg, 2003; Friborg *et al.*, 1997; Jackowicz-Korczyński *et al.*, 2010; Sachs *et al.*, 2008; Sturtevant *et al.*, 2012; Tagesson *et al.*, 2012). On the other hand, profile methods gather the soil gas through tubing inserted into the subsurface layers and measure the GHG concentration at specific depths to calculate flux rates using gas diffusion law (Brummell et al. 2012; Kim et al. 2007; Lee et al. 2010; Miao et al. 2012). For soil samples transported from permafrost sites to laboratories, gas subsamples are collected and analyzed for their gas composition by gas chromatography or some other laboratory equipment (Michaelson *et al.*, 2011; Rasmussen *et al.*, 1993; Wagner *et al.*, 2007). In addition, soil incubation experiments can be conducted under special laboratory conditions taking into account temperature, insolation, aeration, period, moisture and substrate qualities to find any relationship between those environmental parameters and GHG production rate (Lee *et al.*, 2012; Song *et al.*, 2014; Treat *et al.*, 2014; Waldrop *et al.*, 2010).

Based on the results of such measurements and experiments, it has been reported that the current environmental changes at northern high latitudes make surface carbon pools more vulnerable, which can increase the GHG emission. As already mentioned, in the near future, frozen stored carbon would become an additional carbon source to the atmosphere in global carbon cycles (IPCC, 2013). Nevertheless, there are higher levels of uncertainty regarding projections for the exact timing and amount of GHG emission from changing permafrost compared to other carbon pools (Schuur *et al.*, 2015).

Methodologically, there are fundamental problems that may hinder more

accurate calculation of the carbon release from the thawing permafrost. For instance, the eddy covariance tower covers a greater area than the chamber and is more likely to be disturbed by other GHG sources. Because the two methods analyze in-situ GHG emission above the soil surface, they are not sufficient for investigating complex underground processes affecting GHG transport from the deeper soil layers. These methods often overlook the methane burst triggered by ebullition or plant-mediated outgassing, which deviate from regular outward pathways, i.e. diffusion through the soil layer (Elberling *et al.*, 2011; Heyer *et al.*, 2002; Jackowicz-Korczyński *et al.*, 2010; Kim *et al.*, 2013; Sabrekov *et al.*, 2014; Song *et al.*, 2012; Tagesson *et al.*, 2012; Tokida *et al.*, 2009; Zimov *et al.*, 1996). Regarding this, investigating subsurface soils is beneficial in evaluation of such irregular pathways but with some limitations. Although the profile method approaches the subsurface gas pores directly, the tubing might disturb natural transportation of the soil gas. In addition, this method is not appropriate for the collection of gas samples during winter due to the isolation of the soil gas in ground ice structures (Kim *et al.*, 2007; Lee *et al.*, 2010; Miao *et al.*, 2012). Moreover, it would be insufficient to determine GHG distribution without considering soil environmental conditions affecting the activation of soil microbes and their GHG production (Chen *et al.*, 2003). The organic matter decomposition rate (and GHG production rate) may vary with depth as substrate availability, moisture, aeration, pH, and other factors control the microbial activities. In seasonally frozen grounds, temperature variations and freeze/thaw of soil layer can directly inhibit or promote soil microbes to produce CO_2 and CH_4 (Yang et al. 2014; Yu et al. 2007). For soil incubation experiments, small soil fragments and controlled laboratory settings are fundamentally different from natural conditions, which can ignore interruption of gas transport by surrounding soil structures (Beer and Blodau, 2007).

Laboratory gas extraction also has some problems regarding gas leakage and contamination during sample storage and treatments (Lee *et al.*, 2012; Michaelson *et al.*, 2011; Rasmussen *et al.*, 1993; Wagner *et al.*, 2007).

1.1.3 Seasonal GHG outgassing from permafrost

Methane outburst during transitional seasons has been reported in some permafrost regions, which suggests irregular transport of the underground GHG from the subsurface to the atmosphere. According to some chamber observations, a sudden increase in the methane outgassing rate at the onset of soil freezing or thawing was comparable or even larger to the emission during the whole thawed season (Fiborg *et al.*, 1997; Mastepanov *et al.*, 2008; Song *et al.*, 2012; Windsor *et al.*, 1992). This phenomenon is attributable to a physical change of soil layers rather than rapid decomposition activity by soil microbes during such a short period (Brummell *et al.*, 2012).

Fig. 2 shows a schematic diagram for seasonal GHG outgassing pathways through the upper permafrost and the active layer. During summer (from June to August) the whole active layer is thawed and the produced GHG can be transported freely to the atmosphere by several pathways such as diffusion, ebullition (gas bubbles), and plant-mediated transport. The ground temperature decreases rapidly in autumn and the soil layer starts to freeze from the surface. This downward freezing may squeeze out the CH_4 gas stored in pore space or dissolved in soil pore water (Mastepanov *et al.*, 2008). During winter (from November to February or March) the top layer is wholly frozen and covered by snow whilst the deeper part is sometimes not physically frozen (only cryotic; even if temperature is 0°C, the soil layer can remain unfrozen due to salinity effect of pore water). This can promote soil microbes to be activated and produce GHG. In addition, under the frozen and gas impermeable surface, the

remnant GHG fails to release despite the autumn squeezing process. In spring, the surface layer re-opens by thaw and the isolated GHG can be released gradually or sometimes quickly enough to make anomalies in chamber detection (Song *et al.*, 2012; Windsor *et al.*, 1993). Although some studies have been conducted regarding such abnormal flux events during the phase transition of the active layer (Elberling, 2003; Mastepanov et al., 2008; Song et al., 2012; Wang and Wu, 2012; Zimov et al., 1996), whether this event generally occurs through all permafrost regions needs to be more thoroughly investigated (Chang *et al.*, 2012; Jackowicz-Korczyński *et al.*, 2010).

1.2 Vertical profile study

To achieve a robust estimation of GHG release from thawing permafrost, most studies have focused on spatial variability. The surface efflux measurements for soil generated gases are often regarded as representative of the whole underground procedure. For this reason, the detailed emission process has been relatively ignored, which limits a more sophisticated understanding of this newly-recognized carbon source. Therefore, comprehensive investigation of underground soils is necessary to demonstrate where the carbon decomposes and the GHG can be produced within soil columns, and how they can be transported to the atmosphere. Regarding this, establishing vertical profiles seems advantageous not only for deep permafrost as a vestige of long term climate change (Wagner *et al.*, 2007) but also for shallow layers vulnerable to near future warming (Elberling *et al.*, 2013; Harden *et al.*, 2012). A vertical profile of Siberian permafrost core revealed its deposition history since Holocene; the first 4-m layer from the surface was considered to be deposited during the late Holocene and a high concentration of accumulated CH_4 was detected with active microbes (Wagner *et al.*, 2007).

The high CH_4 contents suggest that underground methanogenesis is possible despite low temperatures while the produced methane is trapped within the gas impermeable surroundings. If similar conditions occur in a much shorter time period, i.e. seasonally, the accumulated GHG may be detectable at some depths within the winter soil layers before spring release (Fig. 2).

For explicit parameterization, such seasonality of permafrost GHG emission as in Fig. 2 needs to be precisely evaluated. In the case of temperate wetland regions, there are multiple studies to estimate the net GHG emission using vertical profiles of gas concentration in pore water (Beer and Blodau, 2007; Corbett *et al.*, 2012; Elberling *et al.*, 2011; Tokida *et al.*, 2009; Tokida *et al.*, 2005; Tokida *et al.*, 2007). Similarly, the active layer and permafrost GHG profiles can be analyzed with careful concerns about cryogenic processes and ice structures (Elberling and Brandt, 2003). The gas permeable depth for direct GHG emission can be controlled by the frozen depth of the active layer: shallow during winter, deep during summer, and changeable during spring or autumn, which also modulates the GHG production range in permafrost regions.

1.3 Objectives

Alaska has all latitudinal types of permafrost (see 1.1.1) within various ecological settings such as coastal tundra, boreal forest and peat bog. Since the terrain has received attention for its economic value as an oil field, industrial infrastructure and towns were constructed during the early industrial era (e.g. trans-Alaska pipeline and Alaska Routes). Consequently, the need for scientific observation arose earlier than other permafrost territories because Alaskan people had already suffered from frequent damage to their buildings by ice-rich permafrost thaw (Osterkamp, 2003). Recently, with rising concerns about PCF, Alaska has been emphasized as one of the major high latitudinal carbon stocks

that is vulnerable to climate warming. From 30-year observations, it has been noticed that Alaskan permafrost has already gone through serious changes. A modeling result revealed that the southern part may disappear at the end of this century (Marchenko *et al.*, 2008; Osterkamp, 2003). However, it is not fully understood how degrading permafrost and its stored carbon will respond to future climate change, obstructing more plausible PCF parameterization of this region.

Many investigators have attempted to determine the vulnerability of stored carbon and the probability of increasing GHG emission from various Alaskan soils (Johnston *et al.*, 2014; Kim *et al.*, 2013; 2007; Lee *et al.*, 2012; 2010; Michaelson *et al.*, 2011; Rasmussen *et al.*, 1993; Sturtevant *et al.*, 2012; Treat *et al.*, 2014; Waldrop *et al.*, 2010). Now more comprehensive studies considering physical, chemical and biological components together are needed to understand the simultaneous response of those controlling factors to temperature rise. The aim of this study is to obtain detailed GHG profiles of frozen Alaskan soils so that the gas storage depth may be identified. If there is a high concentration of GHG accumulated in the winter soil profiles, this potentially could result in abrupt spring emission. In order to clarify the GHG production and mobility, soil properties such as organic carbon, nitrogen and water content were evaluated. Borehole temperature profiles were obtained in the field to estimate active layer depth and vertical temperature fluctuations upon seasons. This will be helpful to understand the physical states of certain layers regulating the upward gas transport. Further, all those depth profiles in high resolution can help to improve understanding about greenhouse gas formation and emission through soil layers on Alaskan permafrost region.

2. Materials and Methods

2.1 Sample collection

During the end of the Alaskan winter, soil samples beneath the snow cover were taken with a SIPRE coring auger (3-inches in diameter with PVC liners fitted in the auger), from five locations along the trans-Alaskan pipeline. (Fig. 3). With the exception of TS in the continuous permafrost zone of Alaska, the other four sites belong to the discontinuous zone and might have no permafrost layer directly below (see 1.1.1 for permafrost types). Each sampling site lies in the latitudinal environment of Alaskan permafrost. Site TS denotes tundra near Sag River in the continuous permafrost zone of Alaska. The other four sites are located in discontinuous permafrost zones. Two are in black spruce boreal forests near Yukon River (north and south named as NY and SY in this study), one is in post-fire black spruce forest in Cascaden Ridge (CR), and the other is a forest bog site dominated by Sphagnum moss at Poker Flat Research Range (PF). More information on surface vegetation species, snow thickness, and GPS location can be found in Table 1.

When the soil cores were drilled, TS, NY, and SY were completely frozen from surface to bottom (less than 93 cm), while the top 20–30 cm of PF and the majority of CR were thawed. All soil cores were sealed in transparent PVC liners (90 cm long and 7.6 cm in diameter) with silicon caps and stored in a commercial freezer at the field camp (Wiseman, AK) during the campaign. The samples were transported to cold storage at the University of Alaska, Fairbanks (UAF), and then shipped to the laboratory freezer of Seoul National University (SNU) (< -25℃). During shipping, a temperature logger enclosed with the soil cores showed that the temperature did not reach above -20℃. Each soil core was cut into three longitudinal sections using a diamond blade saw. One section

was used for chemical and physical analyses and the remaining sections were properly wrapped for core section description or additional analyses.

2.2 Temperature logging

After retrieving soil cores, custom-made temperature profilers were installed in the sampling boreholes. They consisted of 12 temperature sensors (TMC20-HD, Onset Comp., USA) and 3 data loggers (U12-008, Onset Comp., USA). The profilers were put into a PVC pipe (2 m long) to prevent disturbance by meteoric water. The empty space of the pipe was filled with sand for effective heat transfer from surrounding soils. The temperature sensors were placed at 5 cm intervals and temperature data at different depths were recorded daily for two years from the date of installation.

2.3 Gas analysis

2.3.1 Headspace gas extraction method

In order to extract gas from frozen soil samples, the longitudinal soil core section was cut into 10–20 cm^3 cuboids from 5–10 cm depth intervals. The top organic layers of PF, CR, and SY cores were excluded because the material was too loose to trap gas inside. For gas extraction and analysis, sampling vials (40 mL EPA vials with open-top screw caps & septa, Wheaton, Millville NJ, USA) were filled with frozen soil fragments, 6M NaCl solution (10 mL for effective degassing and microbial inhibition), and laboratory air in the empty space. After the soil sample was put into the vial, a screw-cap with a rubber septum was fastened immediately and sealed again with aluminum foil tape to minimize gas leakage. A total of 65 vials were labeled as mid-depths from each longitudinal core section. In this way, each of the five cores had a subset of samples

representing 11–15 depths, giving a vertical gas concentration profile. The sample vials were left at 65°C for 30 minutes and then shaken manually for 2 minutes to extract the trapped gas from the soil fragments to the headspace. This is a well-established procedure for extracting pore space gas from permafrost soils or marine sediment samples (Kim *et al.*, 2012b; Rasmussen *et al.*, 1993; RESTEK, 2000; Wagner *et al.*, 2007).

Methane (CH_4) and carbon dioxide (CO_2) concentrations of the headspace gas were measured by injecting 1 mL gas from the vial into an Agilent Technologies 7890A GC system (Fig. 4) with flame ionization and thermal conductivity detectors (Agilent Tech, Santa Clara, CA, USA) at the Korea Institute of Geoscience and Mineral Resources (KIGAM, Daejeon, Korea). The CH_4 and CO_2 mixing ratios were calculated from peak areas by comparing with several standard gases (10.2, 100, 1050 ppm, 1%, 10% for CH_4, and 1%, 10% for CO_2). The manual injection error was less than 1.5% and the preexisting CH_4 or CO_2 in the sampling vials were negligible compared to the gas extracted from soils. The headspace volume was calculated by measuring the non-gaseous part (soil particles + soil water + 10-mL NaCl solution) in the vial. Then, the volume of the thawed soil was determined by subtracting 10 mL (added NaCl solution) from the measured non-gaseous part. Although the calculated volume (the thawed soil in the vial) may differ slightly from that of the original frozen soil (which includes gas pore space with ice structures), the volume-based calculation (gas mole per soil volume) is thought to be more appropriate than a mass-based one (gas mole per soil mass) for depth profiles. If using a mass-based calculation, the gas concentration would be exaggerated in organic layers (e.g. top 70 cm of PF) due to the low density of organic materials. Total uncertainties for the whole procedure were estimated at better than 6.9% for CH_4 and 6.2% for CO_2.

2.3.2 Melting-refreezing gas extraction method

Dry and wet gas extraction from ice core samples (extraction lines equipped with GC systems in Laboratory for Ice Core and Paleoclimate (LICP), SNU) were attempted using archived samples. The dry extraction, requiring no melting of the ice during the extraction, is the proper approach to measure CO_2 concentration because CO_2 has high solubility to liquid water. Clean stainless needles crush the ice under dry vacuum conditions so that the trapped air can be released to the sample tube without CO_2 loss to the meltwater (Ahn *et al.*, 2009). For the wet extraction method, the ice in a sample cup needs to be melted and the trapped air releasd to the cup in a vacuum. Even if the meltwater is refrozen to minimize the solubility effect, this method is more applicable to less soluble gas such as CH_4 than CO_2.

For CO_2 dry extraction, the crushing needles failed to penetrate the Alaskan samples. For CH_4 wet extraction, the melting process without treatment for microbial inhibition offers incubation-like conditions to the soil samples. Thus, the CH_4 mixing ratio comprises both methane primarily trapped within soil and that produced by potential incubation during the warming condition. Presumably, the observed bubbling phenomenon during the melting in the LICP wet extraction line (Fig. 5) indicated there might be some microbial activity, which can change the composition of the naturally trapped gas. On the other hand, the vacuum process using a pump before melting might extract the pore gas trapped in the outer part of the sample, which can lead to lowered CH_4 contents per soil volume (see Appendix).

2.3.3 Supplemental analysis on CH_4

For the three gas samples with high CH_4 concentrations, the stable carbon ($\delta^{13}C_{CH4}$) and hydrogen isotopic ratio (δD_{CH4}) of CH_4 were analyzed by an

isotope ratio mass spectrometer (Isotech, Champaign, IL, USA). The isotopic composition of CH_4 can be used to examine whether the extracted CH_4 was produced by microbial activity in sediments (Anthony *et al.*, 2012; Kim *et al.*, 2012a; Kim *et al.*, 2007; Whiticar, 1999). Also, to check whether the CH_4 was well preserved in the frozen soil during the cutting and bottling process, a supplementary experiment was performed. The CH_4 were extracted from the residual soil fragments that had been kept at -25℃ in plastic bags for 30 days after the first analysis. In this experiment, mercuric chloride (2 mL of 4 mM $HgCl_2$ solution) was injected into the vials to more effectively prevent microbial activity during sediment thaw in a 65°C oven, in case the 6M NaCl treatment alone was insufficient (Tuominen *et al.*, 1994). Results from the 16 samples reveal no statistically significant difference in CH_4 concentrations between the result of supplementary experiment and that of the first analysis ($p = .211$ from the Wilcoxon signed-rank test and $p = .178$ from the paired t-test).

2.4 Soil properties

Soil moisture quantities were measured by weighing the vials before and after drying. Organic carbon (org C, %) and total nitrogen (N, %) contents in the remnant soils were determined by elemental analyzer (FlashEA 1112 Thermo Electron corporation, Waltham, Massachusetts, USA), with an accuracy of ±0.01% at the National Instrumentation Center for Environmental Management (NICEM, Seoul, Korea). Prior to analysis, samples were treated with HCl vapor to eliminate inorganic carbon (Komada *et al.*, 2008).

3. Results

3.1 Characteristics of soil layers

The different layers within the cut sections of the soil cores are described in Fig. 6. Each core has some form of cryogenic structure at various depths as a result of frozen soil pore water (Kanevskiy *et al.,* 2011; Shur *et al.*, 2004). The PF core from the forest bog site (Table 1) contains a 70 cm-thick organic peat layer composed of three layers of, from top to bottom, loosely-packed peat, intermediate peat, and densely-packed peat with cryogenic structure (consisting of layered but discontinuous ice lenses less than 1 cm in length and 1 mm in thickness). The NY and SY cores from black spruce forests include semi-decomposed plant litters in the top layer (~20 cm), and at lower depths mineral soil contents gradually increase with depth. The soil layers also feature the cryogenic structure, implying freezing and cohesion of pore water during winter. In particular, the bottom 80–90 cm of the NY core contains relatively thick and unshaped ice ("ataxitic" according to Kanevskiy *et al.,* 2011), possibly a marker for permafrost initiation depth ("aggradational ice" according to Mackay and Burn, 2002). The CR core consists of two distinctive layers. The top layer contains fire-disturbed organic materials mixed with newly grown plants following the fire event (possibly reed canarygrass; see Table 1 for details). The bottom layer is dominated by mineral soil with a lenticular cryogenic structure, which may have been severely melted by the fire and refrozen later. The TS core from tundra has a greyish soil layer similar to loess deposits. The ice lenses and undecomposed plant roots bounded by greyish sediments at 40–70 cm depth imply post-depositional cryoturbation (French, 2007). The grey color indicates poor drainage conditions (Gleysol, Brady and Weil, 2009), which may be caused by the impermeable permafrost layer under neath.

3.2 General features of measured properties

The soil properties of five soil cores are summarized in Table 2. The PF core has the largest org C, N and moisture contents per soil mass due to the thick organic peat layer, while the TS, NY and SY cores have relatively small amounts of org C, N and water. Although vegetation cover is different between the coastal tundra (TS) and the two black spruce forest sites (NY and SY), the carbon content in the frozen ground is similar over the study areas. The CR core experienced a forest fire in 2010 and the fire may have decreased the amount of organic material in the soil.

The coefficient of variation (CV) was calculated to estimate the scattering degrees along the soil columns (from the mean and standard deviation). The CH_4 concentrations revealed larger degree of scattering than CO_2 as CV values were 21.9–168% for CH_4 and 21.3–72.0% for CO_2 among five cores (Table 2 and Fig. 7). Average CH_4 concentration of the PF (38.1 μmol L^{-1}) and TS (163 μmol L^{-1}) cores is much greater than those of the other three cores (0.64 μmol L^{-1} for CR core, 0.78 μmol L^{-1} for SY core, and 0.86 μmol L^{-1} for NY core), while CO_2 concentrations lie within a relatively narrow range for all five cores (2.07–4.43 mmol L^{-1}, Table 2 and Fig. 7).

The CO_2/CH_4 ratio can be used to examine the relative production ratio between CO_2 and CH_4 and alteration of the ratio after production (e.g., CH_4 oxidation and ebullition loss, Corbett *et al.*, 2012; Hodgkins *et al.*, 2014). Among the five, the TS has the lowest CO_2/CH_4 ratios (Table 2). The low CO_2/CH_4 values may be originated from anaerobic CH_4 production because CO_2/CH_4 values are within the same range as previous anaerobic incubation experiments for 12 sediment samples (both mineral and organic) from permafrost sites in Alaska and Siberia (4–586, Lee *et al.*, 2012). Likewise, the deepest sample of the TS

core (81 cm) has CH_4 values of 0.012 mgC gdw^{-1}_{soil} and CO_2 values of 0.19 mgC gdw^{-1}_{soil} (gdw = gram dry weight), which are comparable to the cumulative amount of CH_4 (~0.026 mgC gdw^{-1}_{soil}) and CO_2 (~0.34 mgC gdw^{-1}_{soil}) from the incubation experiments for 9 mineral soils from Alaskan and Siberian permafrost over 500 days at 15°C (Table 2 in Lee *et al.*, 2012). By contrast, the other three cores (NY, SY and CR) have high CO_2/CH_4 values of 2410–3280 (Table 2). CH_4 content in these cores is much smaller than those from incubation experiments (Lee *et al.*, 2012), while the CO_2 level is in the range of the incubation results. In addition, CO_2 varies over a relatively small range between the five cores. Thus, it can be said that that the high CO_2/CH_4 in NY, SY, and CR cores is attributable to lower CH_4 production than CO_2, probably when the subsurface maintained aerobic conditions. However, if soil conditions are close to anoxia and anaerobic decomposition is favorable, the resulting low CH_4 can arise from high mobility of CH_4 to the atmosphere, possibly by aerenchyma transport or ebullition escape after subsurface production (Corbett *et al.*, 2012; Kim *et al.*, 2007; Tokida *et al.*, 2009). In that case, the trace levels of CH_4 observed in the three cores (NY, SY, and CR) may indicate a lack of CH_4-isolating conditions (e.g. the thick organic layer in the PF core).

3.3 Vertical profiles of CH_4, CO_2 and soil properties

The CH_4, CO_2 and measured soil properties were plotted as depth profiles in Figs. 8 and 9. It is clear, from the first column of Fig. 8 that the methane content sharply increases at certain depth, named as 'CH_4 peak' in this study. The CH_4 profile of PF has a peak at depth of 78 cm (183 ± 13 μmol L^{-1}), and the TS core has two peaks at 27 (416 ± 29 μmol L^{-1}) and 81 cm (331 ± 23 μmol L^{-1}). Such CH_4 peaks were not found in the NY, SY, and CR profiles (Table 2 and Fig. 9). Rather, the CH_4 profiles in Fig. 9 look similar in shape with the CO_2 profiles

in the measured depth ranges. For all the five soil cores, the CO_2 profiles did not reveal any distinctive peak (i.e. significant increase at certain depth) comparable to the CH_4 (Figs. 8 and 9).

Organic carbon, nitrogen and water contents are compared with GHG profiles in Fig. 8. A large portion of organic C in the top 70 cm of PF core (~40%) is attributable to the peat composition, as described previously. The high water content (~60%) may also be attributable to the peat moss because peat moss has a high water-absorbing capacity. Organic carbon and water contents in the PF core decrease sharply below the 70 cm depth as the layer changes to mineral-dominated soils. The TS has a thinner organic layer and the org C, N contents and the C/N ratio disaccord with both the CH_4 and CO_2 concentrations. With the soil layer types in Fig. 6, it appears that there are no particular effects of cryogenic structures on soil org C or N depletion (Fig. 9). Also, for the two boreal forest cores (NY and SY) the water percentage is highest in the top layer due to the water holding capability of organic residues, the water content in the mineral soil layers may reflect the growth of pore ice. Especially, the increase of water percent at a depth of 50 cm in the SY profile matches with the ice-rich part (Figs 6 and 9). There, the CO_2 concentration is lower than the above layer with less ice, which might be resulted from the freezing of the soil pore water with degassing of CO_2 by the lowered solubility in the ice.

3.4 Temperature profiles

Borehole temperatures at the sampling sites (data from the TS site is lacking due to technical problems) were measured in the following year after core sampling (from May 2013 to September 2014). From the temperature data covering the two growing seasons (including temperature maxima from two years), the boundary depth between the active layer and permafrost for sites PF

and NY is estimated at ~70–80 cm. In contrast, the boundary of the SY core appears to not be located within the core depth of 80 cm. The boundary may exist at a deeper depth or may not exist at the site because the SY core is located in the discontinuous permafrost zone of Alaska (Fig. 3). The CR core reveals higher temperatures throughout all depths compared to the other three cores, possibly due to its low latitude and the fire event in 2010.

In the year of 2013, when the cores were drilled, spring was delayed due to a longer previous winter. The average air temperature in April of 2013 was at least 10°C lower than that in April of 2012 and 2014, as reported by weather stations in Bettles, Ester and Fairbanks (locations are marked in Fig. 3; temperature data are available at the Alaska Climate Research Center website: http://akclimate.org/acis_data). The relatively warm air conditions in 2014 compared to 2013 may explain the overall increase in soil temperatures in July 2014 from July 2013, as shown in Fig. 10.

The vertical temperature gradients vary from site to site, which can be attributed to thermal conductivity being dependent on layer composition (French, 2007). Over time, deep soil temperatures gradually approach those of the upper layer (downward freezing and thawing) because atmospheric heat transfer to deep soil lags behind surface temperatures. As a result, the maximum depth of freezing occurs in mid-April (not mid-winter) and that of thawing in late September (not mid-summer). The 20–80 cm soil layers start to freeze from the surface down in October, while some depths remain near 0°C (warmer than surface) for a 1–3 months longer, making tongue-like features in a time series of temperature profiles (light blue areas in Fig. 10). Such phenomena were reported in previous studies and are named the “zero curtain effect” (Outcalt *et al.*, 1990; Romanovsky and Osterkamp, 2000). Even though all subsurface temperature profiles record these tongue-like features during the

winter, the PF core interior appears warmer than the others (in Fig. 10, the light-blue area is more extensive in PF from March to April). This might be due to the thick organic peat layer at the PF surface (Fig. 6), which can chill, or inhibit heat transfer from the surface to deep soil layers (Abu-Hamdeh and Reeder, 2000; Dissanayaka *et al.*, 2012). However, it needs to be considered that many other environmental factors can affect thermal conductivities of soil columns as well as the inherent difference in the air temperature conditions (Brady and Weil, 2009; French, 2007).

4. Discussion

4.1 Confirmation of trapped CH_4

The gas sample extracted from the TS core shows a CH_4 isotopic ratio of δD_{CH4} = -206.6‰ and $\delta^{13}C_{CH4}$ = -68.7‰. The results indicate that the microbial origin of CH_4, according to the informative diagram of Fig. 4 in Whiticar (1999). The other two gas samples from TS and PF have no available δD_{CH4} data due to limited amounts, but the low $\delta^{13}C_{CH4}$ values (-62.5 and -63.0‰ in Fig. 8) may also indicate a bacterial rather than thermogenic origin. Also, it is unknown whether the trapped gas could be conserved well in the frozen soil until extraction although the frozen soil cores were sealed in PVC liners under –25°C. The result of the supplemental experiment (about the archive samples stored for 30 days in the freezer after cutting and treated with $HgCl_2$) showed that the difference in CH_4 results are not statistically significant (see 2.3.3 for detail). Thus, it is concluded that the frozen soil fragment adequately preserves both the concentration of trapped CH_4, without considerable leakage (at least 30 days after cutting), and any extra CH_4 formed during sample treatment for gas extraction.

4.2 Occurrence of "CH_4 peak" in vertical profiles

In Fig. 9, CH_4 peaks occur in lenticular ice layers, but those ice lenses also exist in soil columns in NY, SY and CR cores where CH_4 peaks are not distinct (Fig. 9). Thus, the layered ice is not a sufficient condition for the CH_4 peaks. Nevertheless, for the two CH_4 peak profiles, the discordance with other properties (org C, N, and C/N) may imply that CH_4 peaks are more likely formed by certain physical conditions that limit gas transport rather than chemical properties that govern the overall gas production rate within the soil layer

(Brummell *et al.*, 2012). In contrast, CH_4 peaks are not found in NY, SY, or CR cores (see first column of Fig. 9). Rather, the CH_4 values of these three cores vary within a limited range of 0.2–3.1 μmol L^{-1} and correlate with CO_2 (n = 38, Spearman's rank correlation, $r_s = 0.497$; $p = .002$). In addition, the org C and N contents of the NY, SY, and CR (Fig. 9) appear to positively correlate with CH_4 and CO_2, but only the CO_2 correlation is statistically significant (n=38, Spearman's rank correlation; $r_s = 0.539$, $p < .001$ for CO_2 with org C; $r_s = 0.464$, $p = .003$ for CO_2 with N; $r_s = 0.531$, $p < .001$ for CO_2 with C/N). This positive correlation may reflect that carbon turnover rates are in proportion with the amount of C and N substrates available for microbial activities (Chen *et al.*, 2003; Dubey *et al.*, 2003; Harden *et al.*, 2012; Knoblauch *et al.*, 2013; Lee *et al.*, 2012; Michaelson *et al.*, 2011). Furthermore, the factors affecting vertical gas distribution postulated for CH_4 peaks in PF and TS cores may not be relevant here (Brummell *et al.*, 2012). However, because the quality of the organic matter (i.e. lability of C and N) is also important in determining GHG production in soil layers (Hodgkins et al., 2014; Kim et al., 2012a; Harden *et al.*, 2012; Lee *et al.*, 2012; Michaelson *et al.,* 2011), more sophisticated investigation is needed to confirm the observed correlations for the three cores in this study (see Appendix for more statistics).

4.3 Physical controls on "CH_4 peak" formation and preservation

Upward transportation of CH_4 may be temporarily hindered by physical barriers resulting in the formation of CH_4 peaks observed in our vertical CH_4 profiles as mentioned above. For the CH_4 peak in PF, the surface layer with abundant organic residuals (e.g. Sphagnum mosses) might have acted as a barrier for CH_4 efflux during winter because the organic peat layer can hold a large amount of water which can block the pore space as it freezes (Tokida *et*

al., 2007; Winston *et al.*, 1997; Yang *et al.*, 2014). Moreover, the inversion in vertical temperature from November (tongue-like light blue area in Fig. 10) may have formed the frozen surface while the deeper part remained relatively warm. As mentioned in the result section, the other three cores (NY, SY, and CR) also have such tongue-like figures in the temperature profiles, but they experienced sudden temperature drops to below -2°C from March to April whilst the lower PF layer remained at higher temperatures. The relatively warm lower layer of the PF core, with a frozen gas impermeable surface, may have facilitated anaerobic decomposition and kept the methane produced underground (Elberling *et al.*, 2011; Romanovsky and Osterkamp, 2000; Wagner *et al.*, 2007; Yu *et al.*, 2007; Yang *et al.*, 2014). On the other hand, thawing of the surface peat layer and the resulting high porosity may have allowed the layer to disperse its CH_4 by dissolving the gas in the pore water and transporting it through ebullition (Yang *et al.*, 2014). This process may explain the low concentration of CH_4 in the upper part of the PF (Fig. 8), considering that the upper part was already melted when the PF core was sampled.

Alternatively, the poorly drained conditions of the TS may explain the CH_4 peaks because it implies that the soil is in a favorable condition for anaerobic decomposition of carbon (i.e. methanogenesis), similar to wetland soil columns (Dinsmore *et al.*, 2008; Elberling *et al.*, 2011; Tokida *et al.*, 2007; Yu *et al.*, 2007; Yang *et al.*, 2014). The CH_4 and CO_2 profiles of the TS are comparable to the results of an anaerobic incubation experiment for a saturated wetland column (compare Figure 8b in this study with Figures 4b and 4c in Elberling *et al.*, 2011). The depletion in CH_4 between the two peaks in the TS profile may be explained by partial or temporal aerobic conditions due to the remnant oxygen in plant residuals (Elberling *et al.*, 2011; Tanaka *et al.*, 2007). Thus, the two peaks in the TS CH_4 profile probably formed by anaerobic carbon decomposition within the

gas impermeable layer, free from immediate transport or connection to the atmosphere (Heyer *et al.*, 2002; Kim *et al.*, 2007; Mastepanov *et al.*, 2008; Sturtevant *et al.*, 2012; Yu *et al.*, 2007).

4.3 The fate of the trapped CH_4

Future CH_4 emission from the CH_4 peaks in frozen soil columns will depend on thaw depth during the following warm seasons in the field site (Fig. 11). If the CH_4 peaks exist at permafrost depths, they will be maintained until the permafrost turns into the active layer. Although the temperature data for the TS core was not acquired due to sensor failure, the active layer thickness of TS is likely to be less than 50 cm, in accordance with other sites in that latitude (Mishra and Riley, 2014). If so, the upper CH_4 peak in the TS is in the depth range of the active layer, and the trapped CH_4 will be emitted by surface thaw during the following summer (seasonal trapping). However, the deeper CH_4 peak is located in a permafrost depths, and then the CH_4 peak will be maintained until a severe thaw occurs (perennial trapping). On the other hand, the CH_4 peak at the 78 cm depth of PF is located in a depth between the uppermost permafrost layer and the active layer base (Fig. 11). In the following summer, removal of the CH_4 peak at the PF site will depend on the degree of warming. If the climate gets progressively cooler while sedimentation continues, the CH_4 peak formed in the base of the lower active layer, as in the PF core, will be trapped within the permafrost depth by vertical permafrost growth (Wagner *et al.*, 2007).

5. Conclusion

In this study, heterogeneous distributions of CH_4 were found along vertical profiles of 90 cm-long Alaskan frozen soil cores. Trapped CH_4 can be partially attributed to layer characteristics and seasonal freezing, where a temperature anomaly in the active layer may promote anaerobic carbon decomposition and complicate the emission process. Although sampled cores contain the specific site characteristics of different latitudinal locations in Alaska, samples may not be representative of environmental conditions at that latitude (cf. Kim *et al.*, 2013). Therefore, the cores were compared in the context of the characteristic of each soil column, rather than as representative sites for different latitudes in Alaska. This study should be regarded as the preliminary design for future research to connect the subsurface conditions to GHG efflux from various types of soil found in permafrost regions. Additionally, in this study the seasonal freezing of pore water in the active layers resulted in cryogenic structures similar to ones found in permafrost zones. This shows that the long-term growth of permafrost in cold climates results in the incorporation of the active layer into frozen permafrost. In this regard, it is possible that seasonally trapped CH_4 in the active layer can be incorporated into the near-surface permafrost or even the deepest permafrost during long term cooling. The reverse is also possible upon climate warming, that is, degradation of permafrost and thickening of the active layer. Climate warming would then result in the preferential release of CH_4 previously trapped in the near surface permafrost. Although more quantitative investigation is needed, the repetitive trapping or releasing of CH_4 in accordance with the Earth's climate cycles, could have important effects on atmospheric CH_4 fluctuations.

References

Abu-Hamdeh, N. H., and Reeder, R. C., 2000, Soil thermal conductivity effects of density, moisture, salt concentration, and organic matter: Soil science society of America Journal, v. 64, no. 4, p. 1285-1290.

Ahn, J., Brook, E. J., and Howell, K., 2009, A high-precision method for measurement of paleoatmospheric CO2 in small polar ice samples: Journal of Glaciology, v. 55, no. 191, p. 499-506. DOI: 10.3189/002214309788816731

Anisimov, O., 2007, Potential feedback of thawing permafrost to the global climate system through methane emission: Environmental Research Letters, v. 2, no. 4, p. 045016. DOI: 10.1088/1748-9326/2/4/045016

Anthony, K. M. W., Anthony, P., Grosse, G., and Chanton, J., 2012, Geologic methane seeps along boundaries of Arctic permafrost thaw and melting glaciers: Nature Geoscience, v. 5, no. 6, p. 419-426. DOI: 10.1038/ngeo1480

Beer, J., and Blodau, C., 2007, Transport and thermodynamics constrain belowground carbon turnover in a northern peatland: Geochimica et Cosmochimica Acta, v. 71, no. 12, p. 2989-3002. DOI: 10.1016/j.gca.2007.03.010

Brady, N. C., and Weil, R. R., 2009, Elements of the nature and properties of soils, Prentice Hall.

Brummell, M. E., Farrell, R. E., and Siciliano, S. D., 2012, Greenhouse gas soil production and surface fluxes at a high arctic polar oasis: Soil Biology and Biochemistry, v. 52, p. 1-12. DOI: 10.1016/j.soilbio.2012.03.019

Chang, R. Y., Miller, C. E., Dinardo, S. J., Karion, A., Sweeney, C., Daube, B. C., Henderson, J. M., Mountain, M. E., Eluszkiewicz, J., Miller, J. B., Bruhwiler, L. M., and Wofsy, S. C., 2014, Methane emissions from Alaska in 2012 from CARVE airborne observations: Proc Natl Acad Sci U S A, v. 111, no. 47, p. 16694-16699. DOI: 10.1073/pnas.1412953111

Chen, G., Zhu, H., and Zhang, Y., 2003, Soil microbial activities and carbon and nitrogen fixation: Research in Microbiology, v. 154, no. 6, p. 393-398. DOI: 10.1016/s0923-2508(03)00082-2

Corbett, J. E., Tfaily, M. M., Burdige, D. J., Cooper, W. T., Glaser, P. H., and Chanton, J. P., 2012, Partitioning pathways of CO2 production in peatlands with stable carbon isotopes: Biogeochemistry, v. 114, no. 1-3, p. 327-340. DOI: 10.1007/s10533-012-9813-1

Dinsmore, K. J., Skiba, U. M., Billett, M. F., and Rees, R. M., 2008, Effect of water table on greenhouse gas emissions from peatland mesocosms: Plant and Soil, v. 318, no. 1-2, p. 229-242. DOI: 10.1007/s11104-008-9832-9

Dissanayaka, S. H., Hamamoto, S., Kawamoto, K., Komatsu, T., and Moldrup, P., 2012, Thermal Properties of Peaty Soils: Effects of Liquid-Phase Impedance Factor and Shrinkage: Vadose Zone Journal, v. 11, no. 1, DOI: 10.2136/vzj2011.0092

Dubey, S. K., Singh, A., Watanabe, T., Asakawa, S., Singla, A., Arai, H., and Inubushi, K., 2013, Methane production potential and methanogenic archaeal community structure in tropical irrigated Indian paddy soils: Biology and Fertility of Soils, v. 50, no. 2, p. 369-379. DOI: 10.1007/s00374-013-0858-7

Elberling, B., 2003, Seasonal trends of Soil CO2 dynamics in a soil subject to freezing: Journal of Hydrology, v. 276, no. 1-4, p. 159-175.

Elberling, B., Askaer, L., Jorgensen, C. J., Joensen, H. P., Kuhl, M., Glud, R. N., and Lauritsen, F. R., 2011, Linking soil O2, CO2, and CH4 concentrations in a Wetland soil: implications for CO2 and CH4 fluxes: Environ Sci Technol, v. 45, no. 8, p. 3393-3399. DOI: 10.1021/es103540k

Elberling, B., and Brandt, K. K., 2003, Uncoupling of microbial CO2 production and release in frozen soil and its implications for field studies of arctic C cycling: Soil Biology & Biochemistry, v. 35, no. 2, p. 263-272. DOI: 10.1016/s0038-0717(02)00258-4

Elberling, B., Michelsen, A., Schadel, C., Schuur, E. A. G., Christiansen, H. H., Berg, L., Tamstorf, M. P., and Sigsgaard, C., 2013, Long-term CO2 production following permafrost thaw: Nature Climate Change, v. 3, no. 10, p. 890-894. DOI: 10.1038/nclimate1955

French, H. M., 2007, The Periglacial Environment, 3rd, England, Wiley.

Friborg, T., Christensen, T. R., and Søgaard, H., 1997, Rapid response of greenhouse gas emission to early spring thaw in a subarctic mire as shown by micrometeorological techniques: Geophysical Research Letters, v. 24, no. 23, p. 3061-3064. DOI: 10.1029/97GL03024

Friborg, T., 2003, Siberian wetlands: Where a sink is a source: Geophysical Research Letters, v. 30, no. 21. DOI: 10.1029/2003gl017797

Harden, J. W., Koven, C. D., Ping, C.-L., Hugelius, G., David McGuire, A., Camill, P., Jorgenson, T., Kuhry, P., Michaelson, G. J., O'Donnell, J. A., Schuur, E. A. G., Tarnocai, C., Johnson, K., and Grosse, G., 2012, Field information links permafrost carbon to physical vulnerabilities of thawing: Geophysical Research Letters, v. 39, no. 15, p. L15704. DOI: 10.1029/2012gl051958

Heyer, J., Berger, U., Kuzin, I. L., and Yakovlev, O. N., 2002, Methane emissions from different ecosystem structures of the subarctic tundra in Western Siberia during midsummer and during the thawing period: Tellus, v. 54, no. 3, p. 231-249. DOI: 10.1034/j.1600-0889.2002.01280.x

Hodgkins, S. B., Tfaily, M. M., McCalley, C. K., Logan, T. A., Crill, P. M., Saleska, S. R., Rich, V. I., and Chanton, J. P., 2014, Changes in peat chemistry associated

with permafrost thaw increase greenhouse gas production: Proc Natl Acad Sci USA, v. 111, no. 16, p. 5819-5824. DOI: 10.1073/pnas.1314641111

IPCC, 2013, Climate Change 2013: The Physical Science Basis. Contribution of Working Group I to the Fifth Assessment Report of the Intergovernmental Panel on Climate Change [Stocker, T.F., D. Qin, G.-K. Plattner, M. Tignor, S.K. Allen, J. Boschung, A. Nauels, Y. Xia, V. Bex and P.M. Midgley (eds.)], Cambridge University Press, Cambridge, United Kingdom and New York, USA, p. 1535. DOI:10.1017/CBO9781107415324.

Jackowicz-Korczyński, M., Christensen, T. R., Bäckstrand, K., Crill, P., Friborg, T., Mastepanov, M., and Ström, L., 2010, Annual cycle of methane emission from a subarctic peatland: Journal of Geophysical Research, v. 115, no. G2. DOI: 10.1029/2008jg000913

Johnston, C. E., Ewing, S. A., Harden, J. W., Varner, R. K., Wickland, K. P., Koch, J. C., Fuller, C. C., Manies, K., and Jorgenson, M. T., 2014, Effect of permafrost thaw on CO2 and CH4 exchange in a western Alaska peatland chronosequence: Environmental Research Letters, v. 9, no. 10, p. 085004. DOI: 10.1088/1748-9326/9/8/085004

Jorgenson, M. T., Yoshikawa, K., Kanevskiy, M., Shur, Y., Romanovsky, V., Marchenko, S., Grosse, G., Brown, J., and Jones, B., 2008, Permafrost characteristics of Alaska, Institute of Northern Engineering, University of Alaska Fairbanks.

Kanevskiy, M., Shur, Y., Fortier, D., Jorgenson, M. T., and Stephani, E., 2011, Cryostratigraphy of late Pleistocene syngenetic permafrost (yedoma) in northern Alaska, Itkillik River exposure: Quaternary Research, v. 75, no. 3, p. 584-596. DOI: 10.1016/j.yqres.2010.12.003

Kim, D. G., Vargas, R., Bond-Lamberty, B., and Turetsky, M. R., 2012, Effects of soil rewetting and thawing on soil gas fluxes: a review of current literature and suggestions for future research: Biogeosciences, v. 9, no. 7, p. 2459-2483. DOI: 10.5194/bg-9-2459-2012

Kim, J.-H., Torres, M. E., Choi, J., Bahk, J.-J., Park, M.-H., and Hong, W.-L., 2012, Inferences on gas transport based on molecular and isotopic signatures of gases at acoustic chimneys and background sites in the Ulleung Basin: Organic Geochemistry, v. 43, p. 26-38. DOI: 10.1016/j.orggeochem.2011.11.004

Kim, Y., Kodama, Y., Shim, C., and Kushida, K., 2014, Carbon exchange rates in Polytrichum juniperinum moss of burned black spruce forest in interior Alaska: Polar Science, v. 8, no. 2, p. 146-155. DOI: 10.1016/j.polar.2014.01.003

Kim, Y., Kim, S.-D., Enomoto, H., Kushida, K., Kondoh, M., and Uchida, M., 2013, Latitudinal distribution of soil CO2 efflux and temperature along the

Dalton Highway, Alaska: Polar Science, v. 7, no. 2, p. 162-173. DOI: 10.1016/j.polar.2012.11.002

Kim, Y., Ueyama, M., Nakagawa, F., Tsunogai, U., Harazono, Y., and Tanaka, N., 2007, Assessment of winter fluxes of CO2 and CH4 in boreal forest soils of central Alaska estimated by the profile method and the chamber method: a diagnosis of methane emission and implications for the regional carbon budget: Tellus, v. 59, no. 2, p. 223-233. DOI: 10.1111/j.1600-0889.2006.00233.x

Knoblauch, C., Beer, C., Sosnin, A., Wagner, D., and Pfeiffer, E. M., 2013, Predicting long-term carbon mineralization and trace gas production from thawing permafrost of Northeast Siberia: Glob Chang Biol, v. 19, no. 4, p. 1160-1172. DOI: 10.1111/gcb.12116

Komada, T., Anderson, M. R., and Dorfmeier, C. L., 2008, Carbonate removal from coastal sediments for the determination of organic carbon and its isotopic signatures, δ13C and Δ14C: Comparison of fumigation and direct acidification by hydrochloric acid: Limnology and Oceanography: Methods, v. 6, no. JUN, p. 254-262.

Lee, H., Schuur, E. A. G., Inglett, K. S., Lavoie, M., and Chanton, J. P., 2012, The rate of permafrost carbon release under aerobic and anaerobic conditions and its potential effects on climate: Global Change Biology, v. 18, no. 2, p. 515-527. DOI: 10.1111/j.1365-2486.2011.02519.x

Lee, H., Schuur, E. A. G., and Vogel, J. G., 2010, Soil CO2 production in upland tundra where permafrost is thawing: Journal of Geophysical Research, v. 115, no. G1. DOI: 10.1029/2008jg000906

Mackay, J. R., and Burn, C. R., 2002, The first 20 years (1978-1979 to 1998-1999) of active-layer development, Illisarvik experimental drained lake site, western Arctic coast, Canada1: Canadian Journal of Earth Sciences, v. 39, no. 11, p. 1657-1674. DOI: 10.1139/e02-068

Marchenko, S., Romanovsky, V., and Tipenko, G., 2008, Numerical modeling of spatial permafrost dynamics in Alaska, Proceedings of the ninth international conference on permafrost, Volume 29, p. 1125-1130.

Mastepanov, M., Sigsgaard, C., Dlugokencky, E. J., Houweling, S., Strom, L., Tamstorf, M. P., and Christensen, T. R., 2008, Large tundra methane burst during onset of freezing: Nature, v. 456, no. 7222, p. 628-630. DOI: 10.1038/nature07464

Miao, Y., Song, C., Wang, X., Sun, X., Meng, H., and Sun, L., 2012, Greenhouse gas emissions from different wetlands during the snow-covered season in Northeast China: Atmospheric Environment, v. 62, p. 328-335. DOI: 10.1016/j.atmosenv.2012.08.036

Michaelson, G. J., Ping, C. L., and Jorgenson, M. T., 2011, Methane and carbon dioxide content in eroding permafrost soils along the Beaufort Sea coast,

Alaska: Journal of Geophysical Research, v. 116, no. G1. DOI: 10.1029/2010jg001387

Mishra, U., and Riley, W. J., 2014, Active-Layer Thickness across Alaska: Comparing Observation-Based Estimates with CMIP5 Earth System Model Predictions: Soil Science Society of America Journal, v. 78, no. 3, p. 894. DOI: 10.1088/1748-9326/8/3/035020

Osterkamp, T. E., 2003, Establishing long-term permafrost observatories for active-layer and permafrost investigations in Alaska: 1977-2002: Permafrost and Periglacial Processes, v. 14, no. 4, p. 331-342. DOI: 10.1002/ppp.464

Outcalt, S. I., Nelson, F. E., and Hinkel, K. M., 1990, The Zero-Curtain Effect - Heat and Mass-Transfer across an Isothermal Region in Freezing Soil: Water Resources Research, v. 26, no. 7, p. 1509-1516. DOI: 10.1029/90wr00139

Rasmussen, R. A., Khalil, M. A. K., and Moraes, F., 1993, Permafrost Methane Content .1. Experimental-Data from Sites in Northern Alaska: Chemosphere, v. 26, no. 1-4, p. 591-594. DOI: 10.1016/0045-6535(93)90444-A

RESTEK, 2000, A Technical Guide for Static Headspace Analysis Using GC, *in* Corporation, R., ed.: U.S.A., Restek Corporation, p. 2-15.

Romanovsky, V. E., and Osterkamp, T. E., 2000, Effects of unfrozen water on heat and mass transport processes in the active layer and permafrost: Permafrost and Periglacial Processes, v. 11, no. 3, p. 219-239. DOI: 10.1002/1099-1530(200007/09)11:3<219::AID-PPP352>3.0.CO;2-7

Sabrekov, A. F., Runkle, B. R. K., Glagolev, M. V., Kleptsova, I. E., and Maksyutov, S. S., 2014, Seasonal variability as a source of uncertainty in the West Siberian regional CH4flux upscaling: Environmental Research Letters, v. 9, no. 4, p. 045008. DOI: 10.1088/1748-9326/9/4/045008

Sachs, T., Wille, C., Boike, J., and Kutzbach, L., 2008, Environmental controls on ecosystem-scale CH4emission from polygonal tundra in the Lena River Delta, Siberia: Journal of Geophysical Research, v. 113. p. G00A03, DOI: 10.1029/2007jg000505

Schaefer, K., Lantuit, H., Romanovsky, V. E., Schuur, E. A. G., and Witt, R., 2014, The impact of the permafrost carbon feedback on global climate: Environmental Research Letters, v. 9, no. 8, p. 085003. DOI: 10.1088/1748-9326/9/8/085003

Schaefer, K., Zhang, T., Bruhwiler, L., and Barrett, A. P., 2011, Amount and timing of permafrost carbon release in response to climate warming: Tellus B, v. 63, no. 2, p. 165-180. DOI: 10.1111/j.1600-0889.2011.00527.x

Schuur, E. A., McGuire, A. D., Schadel, C., Grosse, G., Harden, J. W., Hayes, D. J., Hugelius, G., Koven, C. D., Kuhry, P., Lawrence, D. M., Natali, S. M., Olefeldt,

D., Romanovsky, V. E., Schaefer, K., Turetsky, M. R., Treat, C. C., and Vonk, J. E., 2015, Climate change and the permafrost carbon feedback: Nature, v. 520, no. 7546, p. 171-179. DOI: 10.1038/nature14338

Schuur, E. A. G., Bockheim, J., Canadell, J. G., Euskirchen, E., Field, C. B., Goryachkin, S. V., Hagemann, S., Kuhry, P., Lafleur, P. M., Lee, H., Mazhitova, G., Nelson, F. E., Rinke, A., Romanovsky, V. E., Shiklomanov, N., Tarnocai, C., Venevsky, S., Vogel, J. G., and Zimov, S. A., 2008, Vulnerability of permafrost carbon to climate change: Implications for the global carbon cycle: Bioscience, v. 58, no. 8, p. 701-714. DOI: 10.1641/b580807

Shur, Y., French, H., Bray, M., and Anderson, D., 2004, Syngenetic permafrost growth: cryostratigraphic observations from the CRREL Tunnel near Fairbanks, Alaska: Permafrost and Periglacial Processes, v. 15, no. 4, p. 339-347. DOI: 10.1002/ppp.486

Song, C., Wang, X., Miao, Y., Wang, J., Mao, R., and Song, Y., 2014, Effects of permafrost thaw on carbon emissions under aerobic and anaerobic environments in the Great Hing'an Mountains, China: Sci Total Environ, v. 487, p. 604-610. DOI: 10.1016/j.scitotenv.2013.09.083

Song, C., Xu, X., Sun, X., Tian, H., Sun, L., Miao, Y., Wang, X., and Guo, Y., 2012, Large methane emission upon spring thaw from natural wetlands in the northern permafrost region: Environmental Research Letters, v. 7, no. 3, p. 034009. DOI: 10.1088/1748-9326/7/3/034009

Sturtevant, C. S., Oechel, W. C., Zona, D., Kim, Y., and Emerson, C. E., 2012, Soil moisture control over autumn season methane flux, Arctic Coastal Plain of Alaska: Biogeosciences, v. 9, no. 4, p. 1423-1440. DOI: 10.5194/bg-9-1423-2012

Tagesson, T., Mölder, M., Mastepanov, M., Sigsgaard, C., Tamstorf, M. P., Lund, M., Falk, J. M., Lindroth, A., Christensen, T. R., and Ström, L., 2012, Land-atmosphere exchange of methane from soil thawing to soil freezing in a high-Arctic wet tundra ecosystem: Global Change Biology, v. 18, no. 6, p. 1928-1940. DOI: 10.1111/j.1365-2486.2012.02647.x

Tanaka, N., Yutani, K., Aye, T., and Jinadasa, K. B. S. N., 2007, Effect of broken dead culms of Phragmites australis on radial oxygen loss in relation to radiation and temperature: Hydrobiologia, v. 583, no. 1, p. 165-172. DOI: 10.1007/s10750-006-0483-7

Tarnocai, C., Canadell, J. G., Schuur, E. A. G., Kuhry, P., Mazhitova, G., and Zimov, S., 2009, Soil organic carbon pools in the northern circumpolar permafrost region: Global Biogeochemical Cycles, v. 23, no. 2. DOI: 10.1029/2008 gb003327

Tokida, T., Miyazaki, T., and Mizoguchi, M., 2009, Physical controls on ebullition losses of methane from peatlands, v. 184, p. 219-228. DOI: 10.1029/2008gm000805

Tokida, T., Miyazaki, T., Mizoguchi, M., and Seki, K., 2005, In situ accumulation of methane bubbles in a natural wetland soil: European Journal of Soil Science, v. 56, no. 3, p. 389-396. DOI: 10.1111/j.1365-2389.2004.00674.x

Tokida, T., Mizoguchi, M., Miyazaki, T., Kagemoto, A., Nagata, O., and Hatano, R., 2007, Episodic release of methane bubbles from peatland during spring thaw: Chemosphere, v. 70, no. 2, p. 165-171. DOI: 10.1016/j.chemosphere.2007.06.042

Treat, C. C., Wollheim, W. M., Varner, R. K., Grandy, A. S., Talbot, J., and Frolking, S., 2014, Temperature and peat type control CO2 and CH4 production in Alaskan permafrost peats: Global Change Biology, v. 20, no. 8, p. 2674-2686. DOI: 10.1111/gcb.12572

Tuominen, L., Kairesalo, T., and Hartikainen, H., 1994, Comparison of methods for inhibiting bacterial activity in sediment: Appl Environ Microbiol, v. 60, no. 9, p. 3454-3457.

Wagner, D., Gattinger, A., Embacher, A., Pfeiffer, E.-M., Schloter, M., and Lipski, A., 2007, Methanogenic activity and biomass in Holocene permafrost deposits of the Lena Delta, Siberian Arctic and its implication for the global methane budget: Global Change Biology, v. 13, no. 5, p. 1089-1099. DOI: 10.1111/j.1365-2486.2007.01331.x

Waldrop, M. P., Wickland, K. P., White Iii, R., Berhe, A. A., Harden, J. W., and Romanovsky, V. E., 2010, Molecular investigations into a globally important carbon pool: Permafrost-protected carbon in Alaskan soils: Global Change Biology, v. 16, no. 9, p. 2543-2554. DOI: 10.1111/j.1365-2486.2009.02141.x

Wang, J., and Wu, Q., 2012, Annual soil CO2 efflux in a wet meadow during active layer freeze–thaw changes on the Qinghai-Tibet Plateau: Environmental Earth Sciences, v. 69, no. 3, p. 855-862. DOI: 10.1007/s12665-012-1970-y

Whiticar, M. J., 1999, Carbon and hydrogen isotope systematics of bacterial formation and oxidation of methane: Chemical Geology, v. 161, no. 1-3, p. 291-314. DOI: 10.1016/S0009-2541(99)00092-3

Windsor, J., Moore, T. R., and Roulet, N. T., 1992, Episodic fluxes of methane from subarctic fens: Canadian Journal of Soil Science, v. 72, no. 4, p. 441-452. DOI: 10.4141/cjss92-037

Winston, G., Sundquist, E., Stephens, B., and Trumbofe, S., 1997, Winter C02 fluxes in a boreal forest: J Geophys Res, v. 102, no. D24, p. 28795-28804.

Winston, G., Stephens, B., Sundquist, E., Hardy, J., and Davis, R. E., 1995, Seasonal variability in CO2 transport through snow in a boreal forest: IAHS Publications-Series of Proceedings and Reports-Intern Assoc Hydrological Sciences, v. 228, p. 61-70.

Yang, J., Zhou, W., Liu, J., and Hu, X., 2014, Dynamics of greenhouse gas formation in relation to freeze/thaw soil depth in a flooded peat marsh of Northeast China: Soil Biology and Biochemistry, v. 75, p. 202-210. DOI: 10.1016/j.soilbio.2014.04.006

Yu, J., Sun, W., Liu, J., Wang, J., Yang, J., and Meixner, F. X., 2007, Enhanced net formations of nitrous oxide and methane underneath the frozen soil in Sanjiang wetland, northeastern China: Journal of Geophysical Research: Atmospheres, v. 112, p. D07111. DOI: 10.1029/2006JD008025

Zimov, S. A., Davidov, S. P., Voropaev, Y. V., Prosiannikov, S. F., Semiletov, I. P., Chapin, M. C., and Chapin, F. S., 1996, Siberian CO2 efflux in winter as a CO2 source and cause of seasonality in atmospheric CO2: Climatic Change, v. 33, no. 1, p. 111-120. DOI: 10.1007/BF00140516

Table 1 Sampling site information.

Site*	Location °N, °W (masl)	Vegetation	Air Temp† °C		Snow thickness‡ (cm)	Sampling		
			Spring	Winter		Date In 2013	Depth (cm)	ALT§ (cm)
TS	69.7, 148.7 (107)	Tundra near Sag River, with dominant surface vegetation of tussock grass (*Eriophorum vaginatum*), dwarf birch (*Betula glandulosa*), American native willow (*Salix pulchra*), and sedge (*Carex lugens*).	-4.3	-23	~70 (31±6)	May 4	0-84	N.A.
NY	66.1, 151.2 (229)	Black spruce (*Picea mariana*) forest on north of Yukon River, shrubs (*Vaccinium vitis-idaea, Vaccinium uliginosum*) and dwarf birch (*Betula glandulosa*), with a surface lichen layer (*Cladonia rangiferina*).	10.9	-22	~50 (45±11)	May 6	4-93	<80
SY	65.8, 149.6 (361)	Black spruce (*Picea mariana*) forest on south of Yukon River, shrubs (*Ledum palustre, Vaccinium vitis-idaea, Vaccinium uliginosum*) and feather moss (*Pleurozium schreberi*) surface.	7.9	-18	~80 (69±4)	April 29	0-83	>80
CR	65.4, 148.9 (258)	Black spruce trees burned by forest fire in 2010. Reed canarygrass (*Phalaris arundinacea*) is the dominance vegetation at surface.	N.A.	N.A.	~5 (N.A.)	May 10	0-82	>80
PF	65.1, 147.5 (210)	Bogs dominated by peat moss (*Sphagnum* spp.) and feather moss (*Hylocomium splendens*) residing under shrubs (*Ledum groenlandicum, Vaccinium uliginosum, Rubus chamaemorus*) and cotton grass (*Eriophorum vaginatum*).	N.A.	N.A.	~30 (N.A.)	May 9	0-86	<80

*Tundra near Sag River (TS); North of Yukon River (NY); South of Yukon River (SY); Cascaden Ridge (CR); and Poker Flat Research Range (PF) in Alaska
†Air temperatures at sampling sites in the winter season of November to March and in the spring season of April 15 to June 15, during 2010 to 2012. Temperatures are three-year averages (NY site is a two-year average because measurement of the 2011 temperature failed). N.A. denotes not available.
‡Snow cover thickness above surface when the cores were drilled. The numbers in parenthesis are three-year averages during the spring season (April 15-June 15, 2010-2012).
§Active layer thickness (ALT) was estimated by the soil temperature profile at each sampling site (Fig. 3). The depth interval of temperature sensors ranges from 5-10 cm from the surface to 80 or 90 cm depth. The boundary between the active layer and the permafrost is defined by a maximum temperature of 0°C during all measurement periods.

Table 2 Mean and standard deviations ($\mu \pm SD$, 1σ) of soil properties by depth from five Alaskan core samples.

Core site Depth interval	TS (n = 15) 5–81 cm	NY (n = 14) 8–89 cm	SY (n = 13) 15–80 cm	CR (n = 11) 27–79 cm	PF (n = 12) 23–83 cm
CH_4 (μmol L^{-1} soil)*	163 ± 120 (73.6%)	0.86 ± 0.73 (84.9%)	0.78 ± 0.44 (56.4%)	0.64 ± 0.14 (21.9%)	38.1 ± 64.0 (168%)
CO_2 (mmol L^{-1} soil)	4.43 ± 1.22 (27.5%)	2.07 ± 1.49 (72.0%)	2.10 ± 1.22 (58.1%)	2.10 ± 0.57 (27.1%)	2.11 ± 0.45 (21.3%)
CO_2/CH_4† (10^3)	0.06 ± 0.07 (117%)	3.00 ± 1.36 (45.3%)	2.92 ± 1.50 (51.4%)	3.36 ± 0.87 (25.9%)	3.01 ± 3.14 (104%)
Org C (wt%)	6.50 ± 4.90 (75.4%)	5.14 ± 11.24 (219%)	5.28 ± 10.54 (200%)	1.92 ± 0.38 (19.8%)	29.4 ± 15.0 (51.0%)
Nitrogen (wt%)	0.49 ± 0.39 (80.0%)	0.32 ± 0.30 (93.8%)	0.34 ± 0.37 (109%)	0.20 ± 0.03 (15.0%)	1.00 ± 0.57 (57%)
C/N ratio	13.2 ± 2.4 (18.2%)	10.0 ± 7.3 (73.0%)	9.2 ± 8.0 (87.0%)	9.7 ± 0.8 (8.2%)	30.0 ± 12.1 (40.3%)
Water (wt%)	40 ± 17 (42.5%)	31 ± 19 (61.2%)	45 ± 18 (40.0%)	25 ± 5 (20.0%)	78 ± 16 (20.5%)

*The volume (L) represents the thawed-soil volume during gas extraction in vials, during which soil particles settled down and gas pore space was filled with NaCl water.

†Mole ratio of average CO_2 to average CH_4, which is a potential indicator for the degree of CO_2 production from anaerobic organic matter decomposition, in the case that these two greenhouse gases were detected from in-situ anaerobic microbial process (Hodgkins et al., 2014; Corbett et al., 2013).

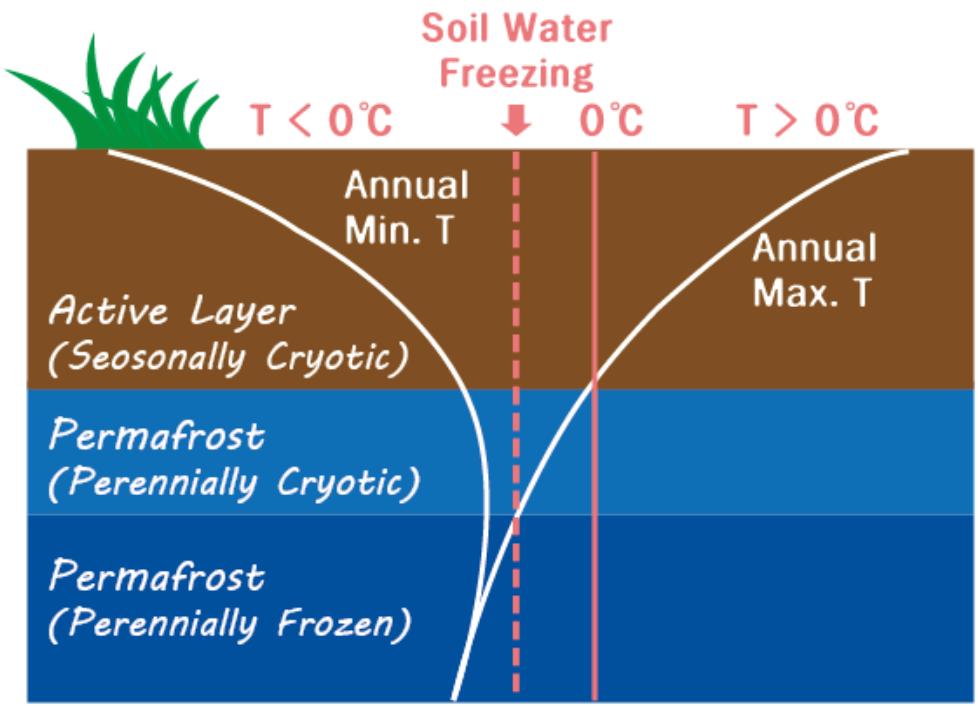

Figure 1 Underground temperature profiles of permafrost area. The top active layer responds to seasonal temperature changes but the permafrost layer below is less affected by the atmospheric temperature change. The permafrost layer can be divided into two parts vertically as perennially cryotic and perennially frozen (French, 2007) since the pore water contains some salts, the freezing temperature is lower than 0℃ (Brady and Weil, 2009).

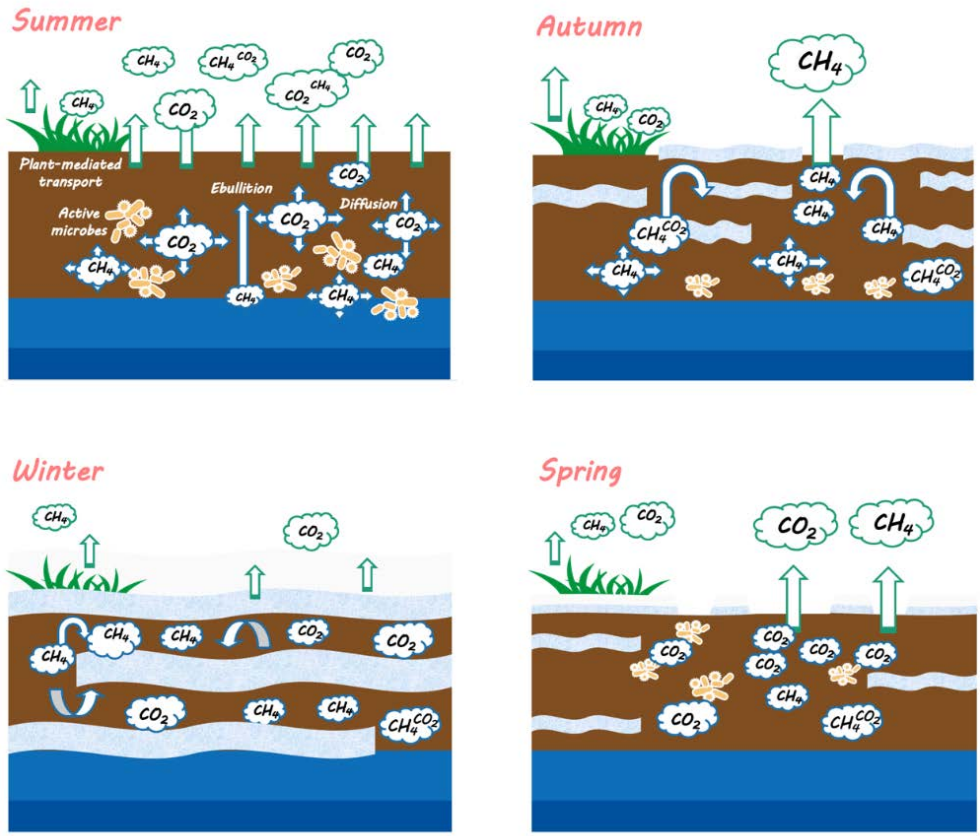

Figure 2 Schematic diagrams for seasonal GHG pathways through soil layers in the permafrost region. In summer, all active layers are in thaw state and freely emitting GHGs by three pathways: diffusion, ebullition and plant-mediated transport. In autumn, when the surface starts to freeze, the GHGs in the pore space or dissolved in pore water can be squeezed out to the atmosphere (Mastepanov *et al.*, 2008). In winter, only limited amount of GHG can be released through frozen soil structures. In spring, soils melt and winter-accumulated GHG might be released at once through the soil columns (Song *et al.*, 2012).

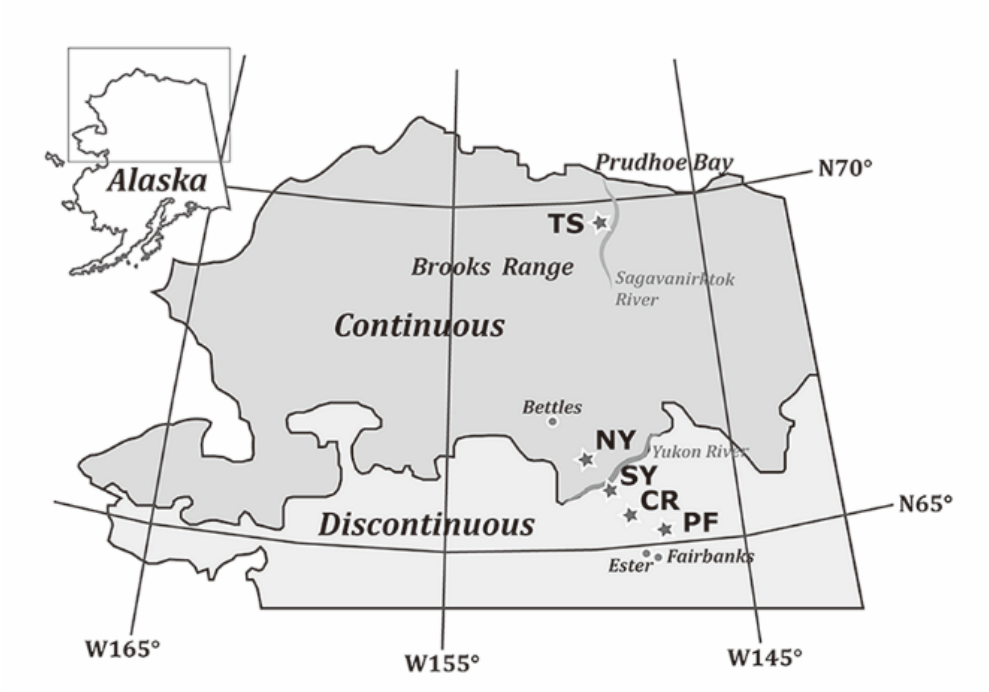

Figure 3 Soil sampling site map. Tundra near Sag River (TS); North of Yukon River (NY); South of Yukon River (SY); Cascaden Ridge (CR); and Poker Flat Research Range (PF) in Alaska. The boundary line between continuous and discontinuous permafrost in the map is adapted from Jorgenson et al. (2008).

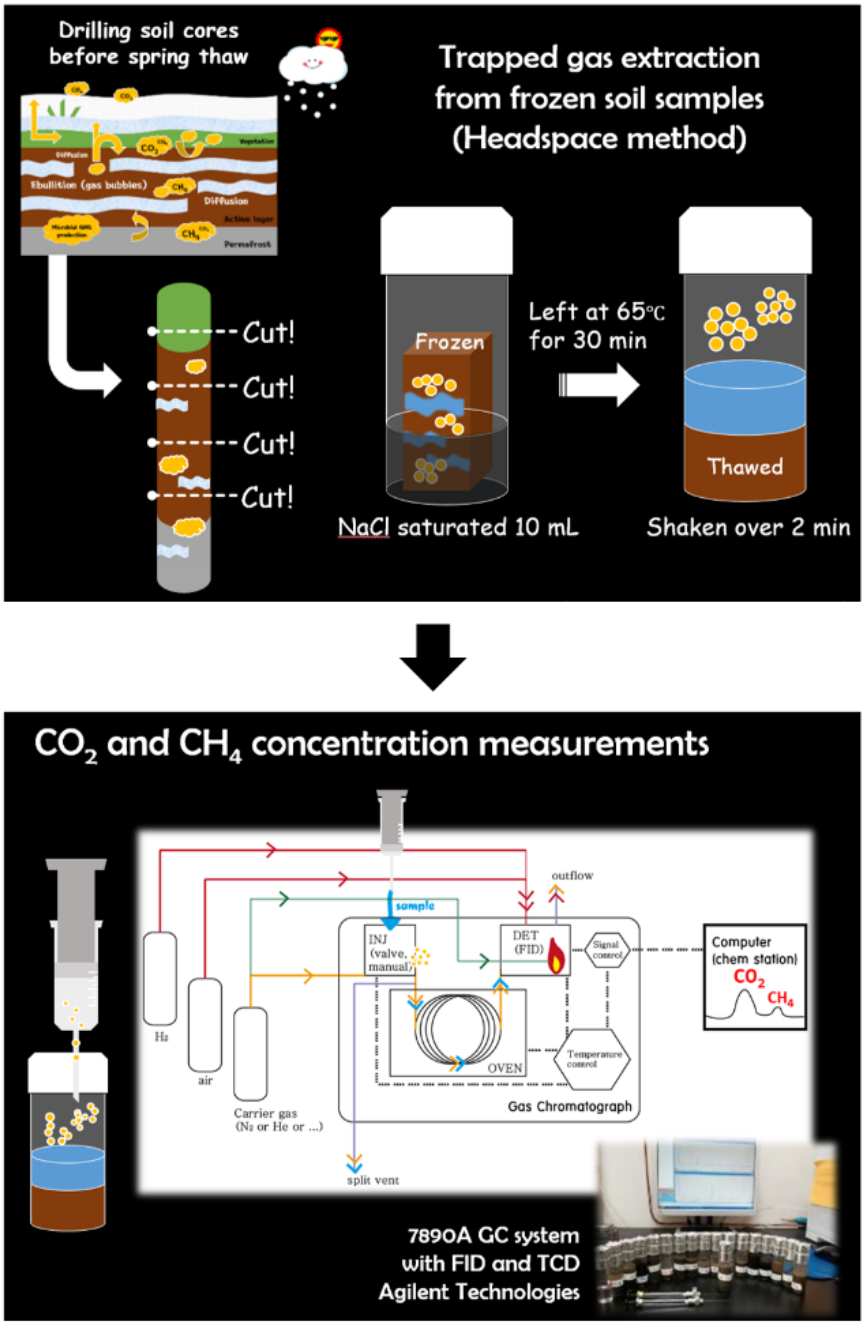

Figure 4 Procedures for the headspace gas extraction and analysis (Kim *et al.*, 2012b; RESTEK, 2000). The concentraion were analyzed by a gas chromatograph (7890A GC system with flame ionization and thermal conductivity detectors; Agilent Tech, Santa Clara, CA, USA) at Korea Institute of Geoscience and Mineral Resources (Daejeon, Korea).

Figure 5 Wet extraction line for CH_4 analysis at Seoul National University. For the analysis, frozen Alaskan soils were put into the sample cups, and then the cups were evacuated. The frozen samples in the cups were melted in a 50°C water bath (about an hour) and refrozen at -80°C ethanol bath to isolate the trapped CH_4 from the solid part of samples. Extracted gases were analyzed by a gas chromatograph system with a flame ionization detector (Agilent Tech GC 7890A, Santa Clara, CA, USA). The picture in the lower right corner shows the bubbling phenomenon during the melting process, which is suspected microbial activity.

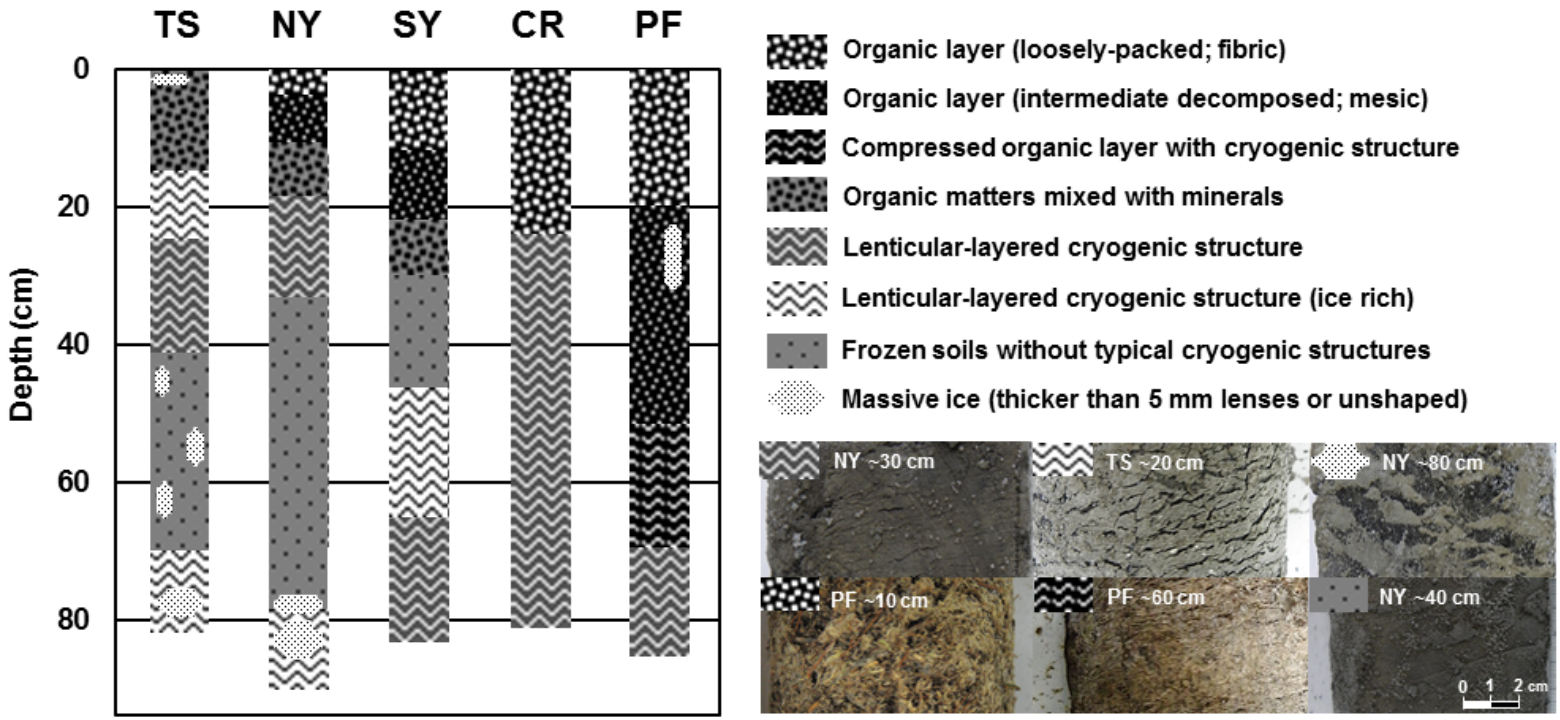

Figure 6 Descriptions of visible sections of the five cores. Each layer is defined by visual observation and simplified into seven soil layer types and one ambiguous structure of ice. "Lenticular-layered cryogenic structures" were named after research on the CRREL permafrost tunnel in Alaska (Shur *et al.*, 2004). More information about sampling sites, including surface vegetation (TS, NY, SY, CR and PF), is listed in Table 1.

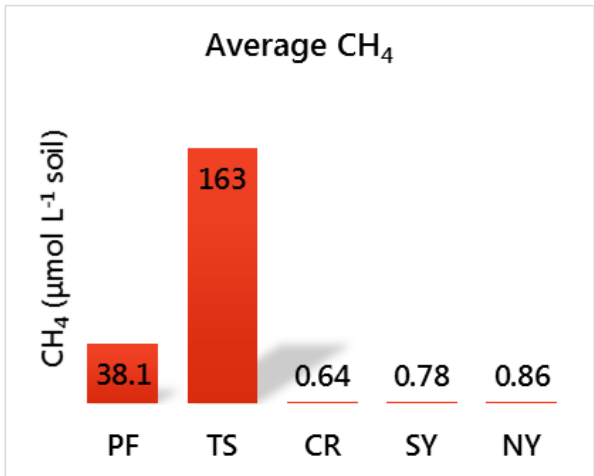

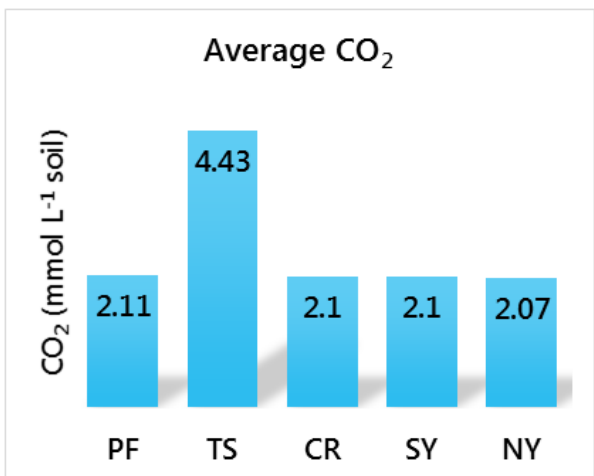

Figure 7 Comparison of average CH_4 and CO_2 contents among five soil cores.

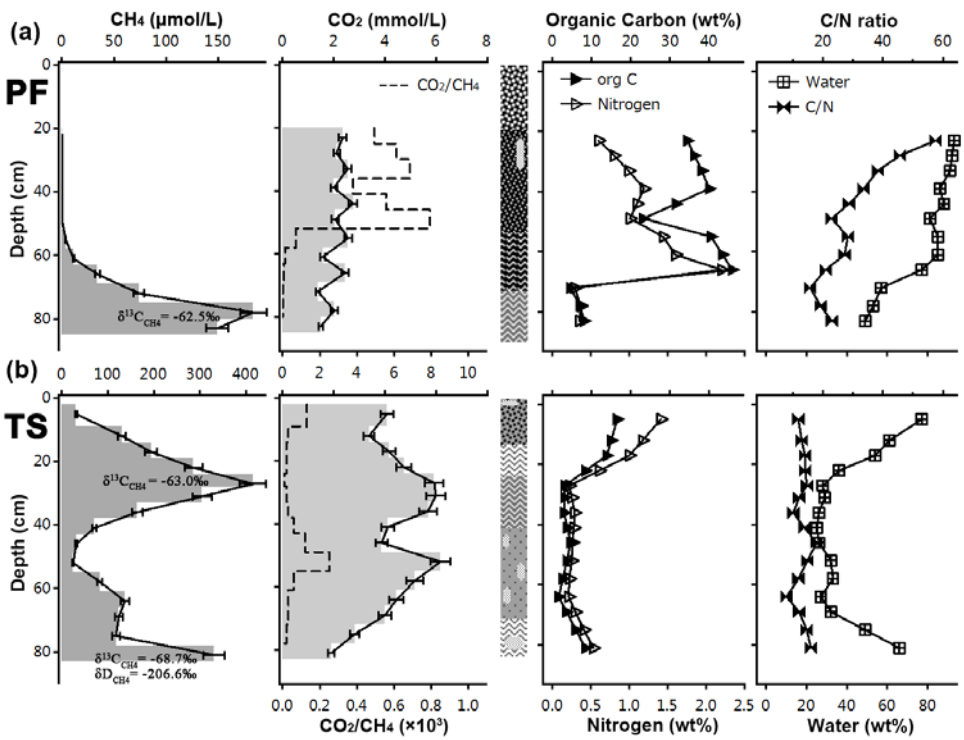

Figure 8 Depth profiles for (a) site PF and (b) site TS. Vertical variation in CH_4 and CO_2 concentrations of thawed soils with calculated CO_2/CH_4 ratios are shown in the first and second columns. Organic carbon, nitrogen and water contents, and C/N ratios are also presented for each depth profile. These two cores include methane concentration peaks below the soil surface and are distinct from the other cores. The carbon and hydrogen isotopic ratios ($\delta^{13}C_{CH4}$ and δD_{CH4}) relative to V-PDB and V-SMOW, respectively, are indicated for each CH_4 peak.

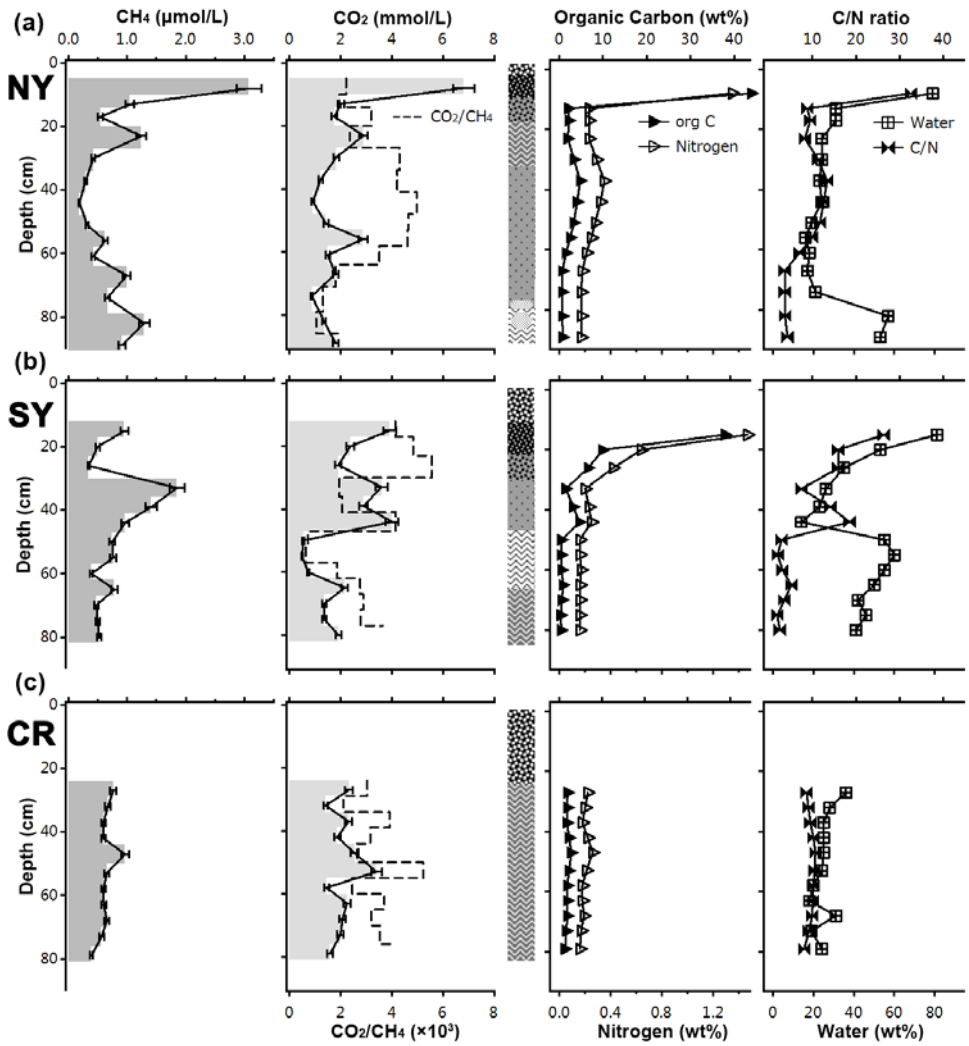

Figure 9 Depth profiles for (a) site NY, (b) site SY and (c) site CR. Vertical variation in CH_4 and CO_2 concentrations of thawed soils with calculated CO_2/CH_4 ratios are shown in the first and second columns. Organic carbon, nitrogen and water contents, and C/N ratios are also presented for each depth profile. These three cores have no methane concentration peaks, contrary to PF and TS cores (Fig. 8). Although CH_4 concentration at the top of the NY core is relatively high, the value is lower than the CH_4 peak concentrations in PF and TS cores by two or three orders of magnitude.

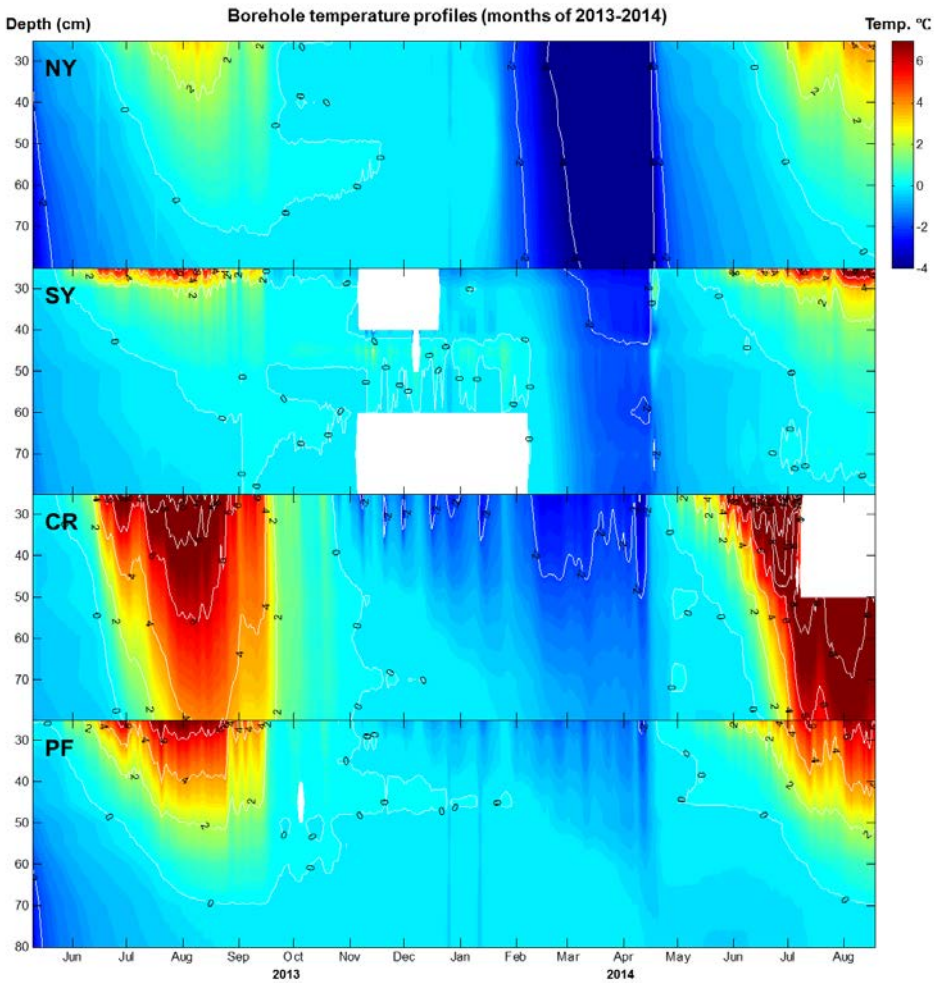

Figure 10 Time series of temperature profiles from the four sampling holes (NY, SY, CR, and PF). The contour plots were made with 0.1 level step by MATLAB R2014a, Mathworks, Massachusetts, USA.

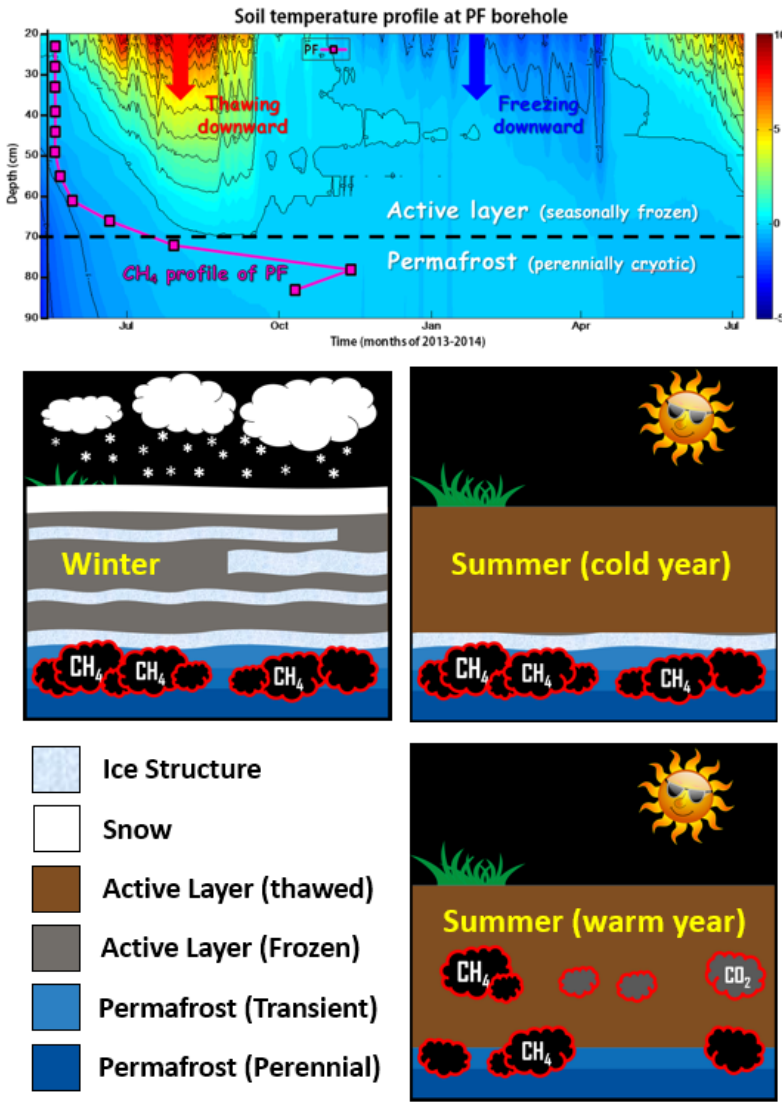

Figure 11 Expected behavior of the trapped CH_4 according to the thawing depth in the following summer (e.g. the case of PF core). The CH_4 peak is located between the active layer bottom and the uppermost part of the permafrost.

국문초록

북반구 고위도 지역의 영구동토는 지난 빙하기 이후 퇴적되어 온 유기물들이 급격히 얼어붙어 분해되지 않은 상태로 저장되어 있다고 알려져 있다. 최근 지구 온난화로 인해 특히 표면 근처 영구동토 층에 저장되어 있던 유기물이 분해될 수 있고 유기물을 구성하던 탄소는 온실기체 형태로 대기 중에 방출될 것이다. 그러나 이러한 현상을 지구 탄소 순환 모델에 포함시키기에는 아직 온실기체 방출량 추정에 불확실성이 높다. 영구동토 지역의 온실기체 방출을 단순히 짧은 기간 동안의 표면 측정 결과에서 추정한다면, 실제 그 지역의 방출 기여도를 과소 또는 과대 평가할 가능성이 있다. 선행연구들에서 지표 아래에 저장되어 있던 유기물의 분해로 인해 생성된 온실기체가 표면 쪽 토양이 얼어붙은 상태에서 기체 투과성이 낮아져 땅 속에 일시적으로 갇혀 있을 수 있다는 보고가 있었다. 이렇게 갇혀 있던 기체들이 토양 층이 다시 녹아 기체 투과성이 회복되면서 급격히 대기 중으로 이동하면, 표면 관측에서 환경 조건에서 예상되는 온실기체 생성을 능가하는 온실기체 방출량이 일시적으로 관찰될 수 있다. 그럼에도 이전의 연구들은 이 같은 이상 방출 현상의 원인이 될 수 있는 땅 속 온실기체 분포 상황에 대해서는 충분히 관심을 가지지 않았다. 이 연구에서는 겨울철 얼어 있는 토양의 온실기체 농도 프로파일이 봄철 토양 표면이 녹으며 나타나는 그러한 일시적인 방출량 증가에 선행한다고 가정하였다. 이를 확인하기 위하여, 2013년 이른 봄 알래스카의 땅이 아직 녹기 전에 위도와 식생이 서로 다른 다섯 곳의 사이트에서 90 센티미터 길이의 코어 샘플을 채취하였다. 샘플에 대해 이산화탄소, 메탄, 그리고 다른 토양 성분들을 약 5에서 10 센티미터 간격으로 측정하여 수직

프로파일로 그려보았다. 흥미롭게도 두 개의 메탄 프로파일에서 특정 깊이의 메탄 함량이 다른 깊이보다 훨씬 높아지는 모양이 관찰되었다. 이것은 앞서 언급한 기체 갇힘 현상의 결과로 나타났을 것이라 생각하였고, 본 연구에서는 편의 상 “메탄 피크” 라고 부르기로 하였다. 이러한 “메탄 피크” 형성에는 토양 층의 온도 역전 현상이 기여하였을 것이다. 토양이 표면부터 얼 때, 상대적으로 따뜻하게 유지된 땅 속 환경에서 미생물 활동이 촉진되어 메탄이 생성될 수 있었을 것이고, 얼어붙은 표면 탓에 생성된 메탄 기체의 방출은 방해를 받아 겨울 내내 땅속에 높은 농도로 남아 있을 수 있었을 것이다. 이렇게 갇혀 있는 메탄이 영구동토 지역 토양 층의 얕은 깊이에 존재할 경우 이듬해 봄 또는 여름철 주변 토양이 녹으면서 쉽게 대기 중으로 방출되거나 산화되어 버릴 수 있을 것이다. 반면에 갇힌 메탄이 더 깊은 곳에 위치하여 이듬해 여름 토양이 최대로 녹는 깊이(활동층 두께)가 갇혀 있는 곳까지 도달하지 못한다면, 토양이 더 깊이 녹을 때까지 여러 해 동안 갇힌 채로 남아 있을 수도 있을 것이다. 이러한 결과들을 생각해 볼 때, 영구동토 지대에서 나타나는 온실기체 방출 현상은 갇힌 메탄의 존재에 의해 더욱 복잡해질 수 있다.

주요 용어 : 영구동토, 온실기체 방출, 활동층, 메탄, 기체 투과성
학번 : 2014-20325

Appendix

A1. Gas and soil properties

Raw data acquired for this study (e.g. vertical profiles in Figs. 8 and 9) are listed in Table A1. The depth, in centimeters, represents the mid-depth of each subsample from the surface in the longitudinal core. The result of melting-refreezing gas extraction at SNU is also presented here. Compared to the CH_4 measured by the headspace method, the results show mostly lowered concentrations (ten out of fifteen measurements), which might be due to the pre-extraction of the open pore gas during the vacuum. Nevertheless, some were observed in higher values, which might be interpreted as microbial activity during the melting process (50°C water bath for more than an hour). Due to these two controversial effects, the measurements of CH_4 by melting-refreezing gas extraction at SNU (see 2.3.2) should not be used for quantitative analysis by direct comparison with the headspace CH_4 data in the study.

Table A1 Measured gas and soil properties from 65 Alaskan samples

Label	Depth (cm)	Water (wt%)	C_{org} (wt%)	N (wt%)	C_{org}/N	CH_4 (μmol/L)	CO_2 (mmol/L)	CO_2/CH_4	pH	CH_4 (μmol/L) at SNU
TS-01	5	77	16.5	1.41	12	30.5	4.08	133	-	31.3
TS-02	12	61	15.0	1.17	13	130	3.38	26	6.4	64.7
TS-03	17	54	13.9	1.00	14	195	4.17	21	6.6	99.8
TS-04	22	36	8.5	0.61	14	286	4.74	17	7.2	184
TS-05	27	28	3.2	0.22	15	416	5.93	14	7.0	-
TS-06	31	30	3.1	0.25	12	305	5.99	20	6.8	-
TS-07	36	26	3.0	0.29	10	164	5.68	35	7.0	-
TS-08	41	25	3.8	0.28	14	70.1	4.11	59	7.0	129
TS-09	46	26	4.7	0.26	18	31.5	3.87	123	7.0	-
TS-10	52	32	3.6	0.25	15	24.6	6.18	252	7.1	-
TS-11	58	33	2.6	0.22	12	82.7	5.17	63	7.1	-
TS-12	64	27	1.6	0.21	8	137	4.45	32	7.0	-
TS-13	69	32	3.6	0.30	12	124	4.00	32	7.1	425
TS-14	75	49	6.0	0.41	15	118	2.82	24	7.5	-
TS-15	81	66	8.4	0.53	16	331	1.90	6	7.1	-
NY-01	8	79	43.9	1.35	33	3.08	6.82	2213	6.0	0.08
NY-02	13	31	2.0	0.23	9	1.04	2.01	1935	6.3	-
NY-03	17	31	2.2	0.23	9	0.54	1.74	3196	6.6	-
NY-04	23	24	1.9	0.23	8	1.24	2.89	2336	6.9	-
NY-05	30	24	3.3	0.29	11	0.42	1.82	4301	7.0	-
NY-06	37	23	4.7	0.35	13	0.30	1.21	4211	7.1	-
NY-07	44	24	4.0	0.32	13	0.18	0.91	4977	7.5	-
NY-08	51	19	3.3	0.28	12	0.31	1.42	4651	7.2	-
NY-09	56	16	2.5	0.25	10	0.62	2.87	4598	7.4	-
NY-10	61	18	1.5	0.21	7	0.42	1.49	3509	7.4	-
NY-11	67	17	0.7	0.18	4	1.00	1.79	1798	7.9	-
NY-12	74	21	0.6	0.17	4	0.66	0.87	1308	7.3	-
NY-13	82	57	0.6	0.17	4	1.30	1.34	1042	8.0	0.15
NY-14	89	53	0.7	0.17	4	0.91	1.79	1966	8.0	-
SY-01	15	81	38.9	1.47	26	0.95	3.91	4135	4.4	-
SY-02	20	53	10.2	0.64	16	0.49	2.37	4831	6.5	-
SY-03	26	35	6.8	0.42	16	0.34	1.90	5556	6.6	2.02

SY-04	33	26	1.5	0.20	8	1.85	3.60	1944	6.9	-
SY-05	39	23	3.2	0.23	14	1.41	2.89	2053	7.4	-
SY-06	44	14	4.7	0.25	18	0.96	4.00	4149	7.5	-
SY-07	50	55	0.5	0.16	3	0.74	0.53	719	-	-
SY-08	55	60	0.3	0.16	2	0.76	0.48	635	7.6	-
SY-09	60	55	0.5	0.17	3	0.39	0.73	1858	8.0	-
SY-10	65	50	0.8	0.16	5	0.78	2.15	2746	8.4	-
SY-11	70	42	0.6	0.16	4	0.47	1.36	2885	8.0	-
SY-12	75	46	0.3	0.16	2	0.49	1.36	2783	8.2	-
SY-13	80	41	0.4	0.16	2	0.52	1.91	3646	8.1	-
CR-01	27	36	1.9	0.22	9	0.76	2.32	3027	-	-
CR-02	32	28	1.8	0.20	9	0.67	1.41	2099	-	-
CR-03	37	25	1.8	0.18	10	0.59	2.30	3913	-	-
CR-04	42	25	2.3	0.22	10	0.59	1.86	3151	-	1.25
CR-05	47	25	2.7	0.26	11	0.96	2.54	2643	-	-
CR-06	53	24	2.2	0.21	10	0.65	3.39	5218	-	-
CR-07	58	20	1.8	0.18	10	0.59	1.45	2448	-	-
CR-08	63	18	1.8	0.18	10	0.60	2.24	3700	-	-
CR-09	68	31	1.8	0.19	10	0.65	2.07	3195	-	-
CR-10	73	19	1.6	0.17	9	0.56	1.99	3529	-	0.33
CR-11	79	24	1.3	0.16	8	0.39	1.58	4065	-	-
PF-01	23	93	34.4	0.60	58	0.47	2.34	4935	4.3	-
PF-02	28	92	36.2	0.80	46	0.35	2.11	6119	4.3	-
PF-03	33	91	38.1	0.99	38	0.37	2.54	6840	4.4	-
PF-04	39	86	40.0	1.19	34	0.53	2.00	3791	4.4	-
PF-05	44	88	31.6	1.10	29	0.49	2.76	5571	4.4	-
PF-06	49	81	23.1	1.01	23	0.26	2.05	7927	4.5	-
PF-07	55	85	40.5	1.44	28	3.63	2.56	706	4.5	-
PF-08	61	85	43.4	1.60	27	11.2	1.57	141	-	-
PF-09	66	77	45.9	2.20	21	34.1	2.44	72	4.7	23.9
PF-10	72	57	4.6	0.29	16	73.9	1.38	19	4.8	43.2
PF-11	78	53	7.0	0.37	19	183	2.02	11	5.5	79.2
PF-12	83	49	8.1	0.35	23	149	1.49	10	5.6	79.0

A2. Statistics

All statistical calculations were performed with IBM SPSS Statistics version 21. The distribution test for organic carbon (C_{org}) and total nitrogen (N) contents reveal that the three boreal forest cores, NY, SY and CR have similar mean concentrations (Kruskal-Wallis test in Table A2). The PF has distinctively large amount of C_{org}, N and water per soil mass because of the thick organic peat layer. The TS only shows conformity with SY water contents. The larger CV values of soil nutrients overall in NY and SY are attributed to relatively well diversified soil horizons from the surface organic layer to the mineral soils below with cryogenic structures, which differentiate the soil properties and possibly the GHGs as well.

Spearman's rank correlation coefficients between soil properties and GHG concentrations are calculated as shown in Table A3. According to the depth profiles (Figs 8 and 9) and the distribution test mentioned above (Table A2), the five core samples were separated into three groups as PF, TS, and the other three (NY, SY and CR) cores without CH_4 peaks (named 'Non-peak'). The statistically significant correlations between CO_2 and CH_4 are only found from the Non-peak ($\rho = 0.497$, $P = .002$). The CO_2/CH_4 ratio is determined by CH_4 variation rather than CO_2 which varies within a relatively small range. CO_2 from the Non-peak tends to decrease by depth as seen from the negative correlation coefficient ($\rho = -0.423$, $P = .008$). In addition, the CO_2 concentrations vary with positive correlations with C_{org} and N contents, though CH_4 has no statistically significant correlation with such properties. The correlations between CO_2 and depth or C_{org} observed in the Non-peak are analogous to the result of coastal frozen soils, Beaufort Sea, Alaska (Michelson *et al.*, 2011). Correlation analysis of the PF and TS shows different tendency from the Non-peak. The CH_4 of PF is negatively correlated with the C/N ratio and %water but positively with depth.

However, the CO_2 of PF has no statistically significant correlation with other properties. Rather, the CO_2/CH_4 ratio of PF is positively related to the C/N ratio and water content, and negatively with the depth. In the TS, the CO_2 has statistically significant correlation with C_{org} and N.

Based on the correlation analysis, multiple linear regression models for GHG distribution are produced (Table A4). To find the largest R^2, the variables were removed or added repeatedly, and the influence of those selected was compared by beta (β) in the selected regression model. The CH_4 in the Non-peak can be most strongly described by CO_2 ($\beta = 0.995$ $P < .001$) among the three variables from a multiple regression model which explains 68.7% of its variation. The CH_4 ($\beta = 0.523$ $P < .001$) and C/N ratio ($\beta = 0.535$ $P < .001$) affected CO_2 variations of the Non-peak to a similar degree in the model ($R^2 = 0.806$, $P < .001$). The %N and depth explained the CO_2 variation of TS by 69.7% ($P = .001$), although the PF had no appropriate regression models for CO_2. A linear model ($R^2 = 0.807$, $P < .001$) with water as the only variable ($\beta = -0.931$, $P < .001$) explains the CH_4 distribution in the PF. Regression models explaining the CO_2/CH_4 were also calculated. Simply, these are explained by CH_4 and CO_2 in the Non-peak and the TS but not in the PF. The CO_2/CH_4 for PF have water as a linear component for its regression model, which the other correlated variables by Spearman's rho are not linear but in some other relationship.

Table A2 Distribution test for the measured values in TS (n=15), NY (n=14), SY (n=13), CR (n=11), and PF (n=12) soil samples by depth. Kruskal-Wallis test is used as a nonparametric method because the number of samples is insufficient to satisfy the normal distribution.

	Null hypothesis (P-value)
Depth (cm)	TS=NY=SY=CR=PF (.756)
CH_4 (μmol L^{-1} soil)	NY=SY=CR (.955)
CO_2 (mmol L^{-1} soil)	NY=SY=CR=PF (.470)
CO_2/CH_4 (10^3)	NY=SY=CR=PF (.900)
C_{org} (wt%)	NY=SY=CR (.452)
N (wt%)	NY=SY=CR (.149)
C/N ratio	NY=SY=CR (.537)
Water (wt%)	TS=SY (.447)

Table A3 Spearman's rank correlation coefficients (ρ) between the GHG concentrations and the measured soil properties in the depth profiles.

	Non-peak (n = 38)			Peak PF (n =12)			Peak TS (n = 15)		
	CH_4	CO_2	CO_2/CH_4	CH_4	CO_2	CO_2/CH_4	CH_4	CO_2	CO_2/CH_4
C	-0.036 (.829)	**0.540*** (< .001)	**0.611** (< .001)	-0.203 (.527)	0.406 (.191)	0.196 (.542)	-0.118 (.676)	**-0.564** (.028)	-0.118 (.676)
N	-0.020 (.905)	**0.462** (.003)	**0.516** (.001)	-0.196 (.542)	0.455 (.138)	0.238 (.457)	-0.018 (.950)	**-0.575** (.025)	-0.157 (.576)
C/N	-0.053 (.753)	**0.531** (.001)	**0.621** (< .001)	**-0.671** (.017)	0.455 (.138)	**0.615** (.033)	0.032 (.909)	-0.246 (.376)	-0.239 (.390)
Water	0.147 (.377)	-0.136 (.414)	**-0.325** (.046)	**-0.769** (.003)	0.517 (.085)	**0.748** (.005)	0.068 (.810)	-0.389 (.152)	-0.243 (.383)
CH_4	1	**0.497** (.002)	**-0.607** (< .001)	1	-0.469 (.124)	**-0.979** (< .001)	1	0.118 (.676)	**-0.921** (< .001)
CO_2	**0.497** (.002)	1	0.292 (.076)	-0.469 (.124)	1	0.538 (.071)	0.118 (.676)	1	0.132 (.639)

*The values in bold are statistically significant spearman's rho ($P < 0.05$), and those in parenthesis are P-values of the coefficients rho (ρ). The correlation coefficients represent any ordinal agreement of two selected variables even if with no linear relationship.

Table A4 Multiple linear regression analysis on the measured values in Table A1.

	Variables						Regression model		
	CH_4	CO_2	%N	C/N	%Water	Depth	R^2	Adjusted R^2	*P*
Non-peak									
CH_4	-	**0.995*** (< .001)	-	**-0.375** (.017)	**0.259** (.013)	-	0.687	0.660	< .001
CO_2	**0.523** (< .001)	-	-	**0.535** (< .001)	-	-	0.806	0.795	< .001
CO_2/CH_4	**-1.286** (< .001)	**0.971** (< .001)	-	**0.254** (.025)	-	-	0.853	0.840	< .001
Peak PF									
CH_4	-	-	-	-	**-0.931** (< .001)	-	0.867	0.854	< .001
CO_2/CH_4	-	-	-	-	-	**-0.806** (.002)	0.650	0.615	.002
Peak TS									
CO_2	-	-	**-0.986** (< .001)	-	-	**-0.964** (.001)	0.697	0.647	.001
CO_2/CH_4	**-0.749** (< .001)	**0.987** (.001)	-	**0.479** (.005)	**0.569** (.016)	**0.346** (.061)	0.867	0.792	.001

*The values in bold and in the parenthesis are beta (β) and *P*-values from the linear regression model about CH_4, CO_2 and CO_2/CH_4 depth distribution with different variables in each non-peak or peak case.

A3. Microbial analysis

Using the FastDNA™ SPIN Kit for Soil (MP Biomedicals, OH, USA), total genomic DNA in the soil was extracted from 0.01 to 0.8 g of freeze-dried subsamples from the four Alaskan soil cores (TS, NY, SY and PF). Following the enclosed protocol, the total gDNA was efficiently isolated for informative analysis for microbial communities using sequencing and the polymerase chain reaction (PCR). Before this, the eluted DNA was visualized through agarose gel electrophoresis and roughly quantified by spectrophotometer for DNA dilution. The resulting bands in the gel electrophoresis (Fig. A1) were smudged because the sample contained many different DNA sources from the soil, including not only soil bacteria or archaea but also plant residuals. Similarly, the DNA quantification through spectrophotometry was not able to infer the microbial quantity of the bulk sample. Instead, microbial abundance and community structures were evaluated by MiSeq sequencing with reference genome and quantitative PCR targeting 16S rRNA gene (by virtue of Dr. Kim, Mincheol and Dr. Lee, Yoo Kyung at Korea Polar Research Institute). Microbial structures were arranged by soil sampling sites and described as depth profiles in Fig. A2.

All of the investigated soil cores comprise bacterial phyla commonly found in permafrost soils such as Actinobacteria, Chloroflexi, Acidobacteria and Proteobacteria (Jansson and Tas, 2014). The bacterial and archaeal communities indicate site specific characteristics, while two soil cores from the site NY and SY show comparable structures with each other. This might be because those two sites are located nearby and share similar environmental conditions like vegetation, temperature and precipitation. There are no depth-induced changes in both two. On the other hand, PF and TS, reveal dramatic shifts in bacterial sequences near permafrost starting depth. The relative

abundance of Chloroflexi in TS is largely decreased, while Caldiserica and Firmicutes significantly increased at depths of >58 cm. Below 72 cm depth in the PF core, Verrcomicrobia and Planctomycetes recede greatly, while Chloroflexi and candidate phylum AD3 increase dramatically. AD3 was found recently from upland boreal forest site in Alaska and does not have cultured-representatives yet (so it is still a 'candidate' phylum; Jansson and Tas, 2014; Tas et al., 2014). Similarly, the Chloroflexi phylum has been commonly found in permafrost soils, but it has few cultured representatives (Jansson and Tas, 2014). Such vertical variations in microbial sequences will be applicable to predict how soil microbes respond to active layer deepening. As spatial heterogeneities are important across various permafrost sites (with different environmental conditions), vertical characteristics need to be well understood considering the phase transition that occurs in the active layer–permafrost interface by global climate change.

References

Jansson, J. K., and Tas, N., 2014, The microbial ecology of permafrost: Nat Rev Micro, v. 12, no. 6, p. 414-425. DOI: 10.1038/nrmicro3262

Tas, N., Prestat, E., McFarland, J. W., Wickland, K. P., Knight, R., Berhe, A. A., Jorgenson, T., Waldrop, M. P., and Jansson, J. K., 2014, Impact of fire on active layer and permafrost microbial communities and metagenomes in an upland Alaskan boreal forest: ISME J, v. 8, no. 9, p. 1904-1919. DOI: 10.1038/ismej.2014.36

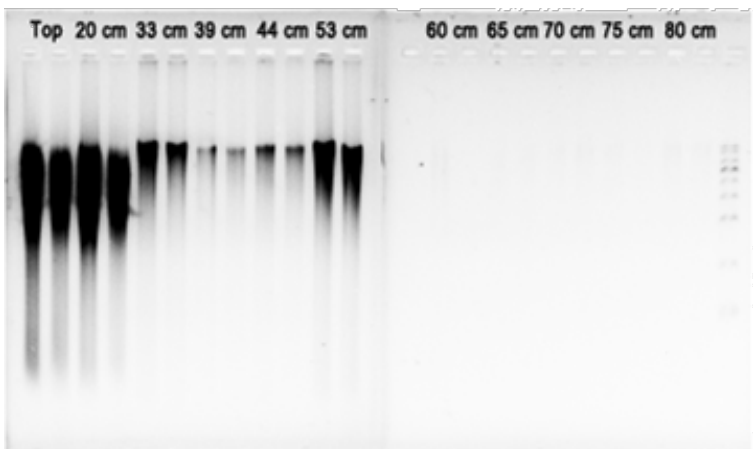

Figure A1 Agarose gel electrophoresis of DNA samples extracted from SY soil core by depth. Digital image was obtained by inverting colors in Photoshop CS6 after taking photograph of the gel under UV light.

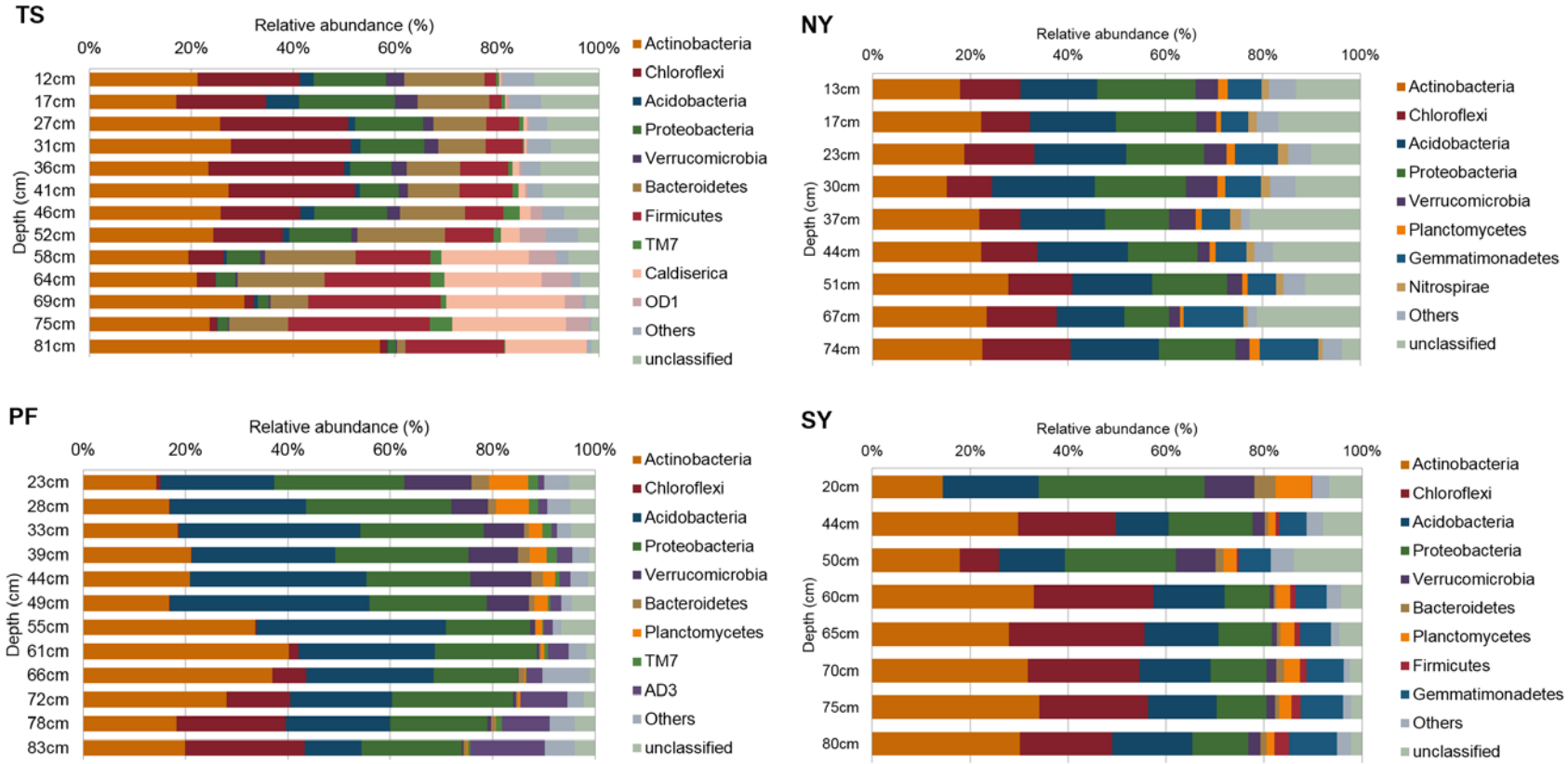

Figure A2 Phylum-level diversities in bacterial community from four core samples.

A4. Geochemical Analysis

For the residual parts of the Alaskan soil core samples preserved in the laboratory freezer (< –25℃), geochemical analysis was conducted focusing on organic matter quantities using Rock-Eval 6 and CHN 900 at the Korean Institute of Geoscience and Mineral Resources (KIGAM, Daejeon, Korea; by virtue of Dr. Kim, Ji-Hoon). Additionally, stable carbon and nitrogen isotope ratios ($\delta^{13}C$ and $\delta^{15}N$) were also analyzed at the National Instrumentation Center for Environmental Management (NICEM, Seoul National University, Korea). The results are listed in Table A5 and A6, and plotted in informative diagrams (Figs. A3 and A4) (Kim et al., 2007; Lamb et al., 2006). Both diagrams suggest that the organic compounds in the soil core samples were mainly originated from land vegetation.

References

Kim, J.-H., Park, M.-H., Tsunogai, U., Cheong, T.-J., Ryu, B.-J., Lee, Y.-J., Han, H.-C., Oh, J.-H., and Chang, H.-W., 2007, Geochemical characterization of the organic matter, pore water constituents and shallow methane gas in the eastern part of the Ulleung Basin, East Sea (Japan Sea): Island Arc, v. 16, no. 1, p. 93-104. DOI: 10.1111/j.1440-1738.2007.00560.x

Lafargue, E., Marquis, F., and Pillot, D., 1998, Rock-Eval 6 applications in hydrocarbon exploration, production, and soil contamination studies: Oil & Gas Science and Technology, v. 53, no. 4, p. 421-437. DOI: 10.2516/ogst:1998036

Lamb, A. L., Wilson, G. P., and Leng, M. J., 2006, A review of coastal palaeoclimate and relative sea-level reconstructions using δ13C and C/N ratios in organic material: Earth-Science Reviews, v. 75, no. 1-4, p. 29-57. DOI: 10.1016/j.earscirev.2005.10.003

Table A5 Results of Rock-Eval analysis at KIGAM

Label*	Depth (cm)	Soil (mg)	S_1† (mgHC /gSoil)	S_2 (mgHC /gSoil)	S_3 ($mgCO_2$ /gSoil)	T_{max}‡ (℃)	HI§ (mgHC /gTOC)	OI ($mgCO_2$ /gTOC)	PC (wt%)	RC (wt%)	TOC (wt%)
TS-01a	5	60	26.51	38.34	33.16	326	234	202	6.7	9.7	16.4
TS-02a	12	61	12.00	45.23	20.55	430	360	164	5.6	6.9	12.6
TS-03a	17	61	8.30	28.17	16.64	322	318	188	3.7	5.1	8.9
TS-05a	27	67	2.78	12.91	4.02	434	436	136	1.5	1.5	3.0
TS-06a	31	67	2.07	10.45	4.49	431	391	168	1.2	1.4	2.7
TS-07a	36	62	1.89	10.00	5.12	429	364	186	1.2	1.6	2.8
TS-08a	41	61	2.12	10.61	5.78	430	355	193	1.3	1.7	3.0
TS-09a	46	60	1.49	7.83	5.36	428	320	219	1.0	1.5	2.5
TS-10a	52	66	5.30	21.28	11.22	431	344	181	2.7	3.5	6.2
TS-11a	58	61	2.95	12.52	7.31	430	337	197	1.6	2.1	3.7
TS-12a	64	62	1.63	8.41	6.04	428	310	223	1.1	1.6	2.7
TS-13a	69	66	0.73	5.26	4.98	426	277	262	0.7	1.2	1.9
TS-14a	75	65	0.06	0.86	5.06	413	101	595	0.3	0.6	0.9
TS-15a	81	63	0.05	0.47	3.87	420	71	586	0.2	0.5	0.7
NY-02a	13	68	0.26	2.38	6.79	423	93	264	0.5	2.1	2.6
NY-03a	17	64	0.27	2.57	7.47	423	92	267	0.5	2.3	2.8
NY-04a	23	67	0.17	1.76	5.39	421	84	257	0.4	1.7	2.1
NY-05a	30	73	0.32	3.37	8.89	421	95	251	0.7	2.9	3.5
NY-06a	37	64	0.29	2.69	7.81	422	92	267	0.6	2.4	2.9
NY-07a	44	58	0.10	1.08	3.83	427	76	268	0.3	1.2	1.4
NY-08a	51	63	0.22	2.33	6.69	423	79	227	0.5	2.5	3.0
NY-09a	56	60	0.59	5.46	10.79	430	122	241	1.0	3.5	4.5
NY-11a	67	65	0.04	0.41	2.10	438	80	412	0.1	0.4	0.5
NY-12a	74	63	0.04	0.40	1.88	432	91	427	0.1	0.3	0.4
SY-02a	20	56	6.30	28.94	24.97	430	255	220	4.0	7.4	11.3
SY-04a	33	63	0.28	2.37	5.62	426	108	257	0.4	1.8	2.2
SY-05a	39	63	0.10	0.60	2.96	422	63	312	0.2	0.8	1.0
SY-06a	44	62	0.13	0.99	3.86	422	75	292	0.2	1.1	1.3
SY-07a	50	57	1.58	9.41	14.58	431	163	253	1.5	4.3	5.8
SY-09a	60	62	0.06	0.15	1.51	430	58	581	0.1	0.2	0.3
SY-10a	65	63	0.05	0.12	1.34	370	55	609	0.1	0.2	0.2

SY-11a	70	61	0.05	0.19	1.41	437	76	564	0.1	0.2	0.3
SY-12a	75	62	0.05	0.17	1.33	358	68	532	0.1	0.2	0.3
SY-13a	80	65	0.05	0.20	1.53	366	74	567	0.1	0.2	0.3
CR-01a	27	60	0.14	1.24	4.39	419	79	281	0.3	1.3	1.6
CR-02a	32	67	0.09	0.86	3.66	421	72	305	0.2	1.0	1.2
CR-03a	37	60	0.11	1.11	4.69	420	71	299	0.3	1.3	1.6
CR-05a	47	61	0.75	6.25	11.08	425	135	239	1.0	3.6	4.6
CR-07a	58	62	0.15	1.81	4.15	423	108	249	0.3	1.4	1.7
CR-08a	63	65	0.10	0.91	3.37	401	81	301	0.2	0.9	1.1
CR-09a	68	66	0.12	1.65	3.08	424	131	244	0.3	1.0	1.3
PF-01a	23	15	48.37	69.75	85.23	300	215	263	13.8	18.6	32.4
PF-02a	28	16	42.85	61.97	93.29	300	202	304	12.9	17.7	30.6
PF-03a	33	15	45.21	72.08	88.83	300	235	290	13.7	17.0	30.7
PF-04a	39	13	48.14	64.76	94.93	300	204	299	13.8	18.0	31.8
PF-05a	44	15	50.89	65.12	90.43	300	209	290	14.0	17.2	31.2
PF-06a	49	14	55.01	70.71	87.24	300	234	289	14.6	15.6	30.2
PF-07a	55	19	52.53	110.13	63.81	317	319	185	16.5	17.9	34.5
PF-08a	61	16	50.58	104.98	73.57	300	319	223	16.4	16.6	33.0
PF-09a	66	13	50.23	145.98	64.54	323	368	163	19.4	20.3	39.7
PF-10a	72	65	17.07	63.76	23.18	426	404	147	7.7	8.1	15.8
PF-11a	78	62	6.02	27.26	8.84	434	414	134	3.2	3.4	6.6
PF-12a	83	62	7.16	32.64	9.94	434	421	128	3.8	4.0	7.8

*****Samples are labelled with 'a' at the end to distinguish them from the earlier samples that had been used for gas analysis.

†S_1, S_2 and S_3: Peaks detected during pyrolysis by Rock Eval 6. S_1 peak denotes the quantity of free hydrocarbons present in the sample; S_2 and S_3 indicate the amount of hydrocarbons and that of CO_2 respectively produced during the thermal cracking of the insoluble organic matter

‡Temperature for the maximum S_2 peak

§HI: Hydrogen index; OI: Oxygen index; PC: Pyrolyzed carbon; RC: Residual carbon; TOC: Total organic carbon.

See reference Lafargue et al. (1998) for details.

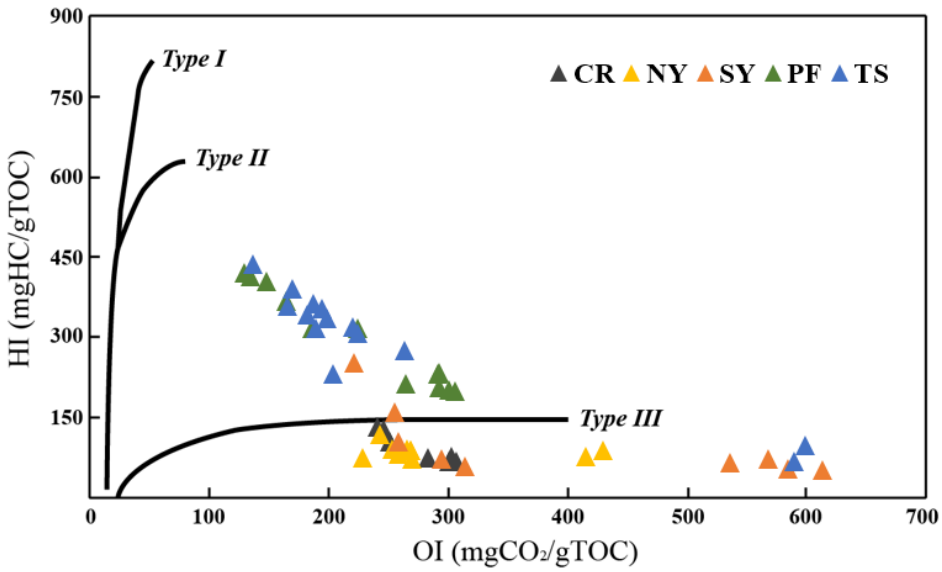

Figure A3 Modified Van Krevelen Diagram (Kim *et al.*, 2007). Type III path indicates land-derived organic matter.

Table A6 Chemical analysis for C and N in organic compounds in the soil samples.

Label*	Depth (cm)	TOC (wt%) Rock-Eval KIGAM	TC (wt%) NICEM	$\delta 13C_{PDB}$ NICEM	TN (wt%) NICEM	$\delta 15N_{AIR}$ NICEM	TC (wt%) CHN900 KIGAM	TN (wt%) CHN900 KIGAM	$TOC_{R\text{-}E}/TN_{CHN}$ KIGAM
TS-01a	5	16.39	15.6	-27.7	1.49	1.8	17.7	1.00	16
TS-02a	12	12.55	-	-	-	-	14.4	0.78	16
TS-03a	17	8.86	5.9	-27.3	0.48	2.2	10.9	0.59	15
TS-05a	27	2.96	2.9	-27.6	0.20	1.0	4.7	0.21	14
TS-06a	31	2.67	-	-	-	-	4.6	0.16	17
TS-07a	36	2.75	-	-	-	-	5.0	0.20	14
TS-08a	41	2.99	3.0	-27.5	0.21	1.0	5.4	0.19	15
TS-09a	46	2.45	-	-	-	-	5.2	0.18	14
TS-10a	52	6.19	9.5	-28.2	0.43	1.1	8.0	0.40	15
TS-11a	58	3.72	-	-	-	-	6.0	0.25	15
TS-12a	64	2.71	2.8	-27.6	0.21	1.7	5.3	0.21	13
TS-13a	69	1.9	-	-	-	-	5.1	0.14	14
TS-14a	75	0.85	1.0	-26.5	0.10	1.8	4.2	0.11	8
TS-15a	81	0.66	0.9	-25.9	0.09	1.7	4.0	0.06	10
NY-02a	13	2.57	-	-	-	-	16.2	0.44	6
NY-03a	17	2.8	2.9	-25.3	0.24	4.1	8.1	0.34	8
NY-04a	23	2.1	-	-	-	-	2.8	0.16	13
NY-05a	30	3.54	-	-	-	-	3.8	0.24	15
NY-06a	37	2.93	3.6	-25.3	0.27	3.9	3.2	0.17	17
NY-07a	44	1.43	-	-	-	-	1.5	0.16	9
NY-08a	51	2.95	-	-	-	-	2.9	0.17	17
NY-09a	56	4.48	-	-	-	-	4.9	0.25	18
NY-11a	67	0.51	0.6	-24.8	0.11	1.8	1.2	0.13	4
NY-12a	74	0.44	-	-	-	-	1.0	0.09	5
SY-02a	20	11.33	10.9	-24.6	0.62	4.1	13.0	0.54	21
SY-04a	33	2.19	2.0	-25.4	0.15	2.7	2.7	0.14	16
SY-05a	39	0.95	-	-	-	-	1.2	0.10	10
SY-06a	44	1.32	1.5	-25.6	0.11	3.8	1.5	0.10	13
SY-07a	50	5.77	6.2	-26.0	0.36	3.2	6.0	0.24	24
SY-09a	60	0.26	-	-	-	-	1.2	0.05	5

SY-10a	65	0.22	-	-	-	-	1.2	0.05	4
SY-11a	70	0.25	-	-	-	-	1.1	0.05	5
SY-12a	75	0.25	-	-	-	-	1.2	0.05	5
SY-13a	80	0.27	-	-	-	-	1.1	0.06	4
CR-01a	27	1.56	1.6	-25.3	0.16	2.9	1.7	0.08	20
CR-02a	32	1.2	-	-	-	-	1.4	0.12	10
CR-03a	37	1.57	-	-	-	-	1.7	0.11	14
CR-05a	47	4.63	5.2	-25.7	0.35	3.5	5.1	0.27	17
CR-07a	58	1.67	-	-	-	-	1.8	0.13	13
CR-08a	63	1.12	-	-	-	-	1.2	0.10	11
CR-09a	68	1.26	1.3	-26.3	0.12	2.0	1.7	0.10	13
PF-01a	23	32.43	43.6	-27.3	1.02	-1.7	36.9	0.47	69
PF-02a	28	30.64	-	-	-	-	39.5	0.52	59
PF-03a	33	30.65	43.4	-26.0	1.39	-1.0	39.9	0.55	55
PF-04a	39	31.76	-	-	-	-	44.0	0.63	51
PF-05a	44	31.16	43.7	-25.7	1.29	-2.6	40.2	0.59	53
PF-06a	49	30.19	-	-	-	-	39.8	0.68	44
PF-07a	55	34.47	-	-	-	-	38.4	1.24	28
PF-08a	61	32.96	45.1	-26.1	2.00	-1.8	44.2	1.22	27
PF-09a	66	39.68	-	-	-	-	40.8	1.56	25
PF-10a	72	15.78	14.8	-26.0	0.95	-0.9	22.5	0.72	22
PF-11a	78	6.58	6.0	-27.0	0.26	2.0	7.3	0.25	27
PF-12a	83	7.76	9.4	-26.8	0.44	1.3	7.9	0.28	28

*Samples were labelled with ‘a’ at the end to distinguish from the earlier samples that had been used for gas analysis.

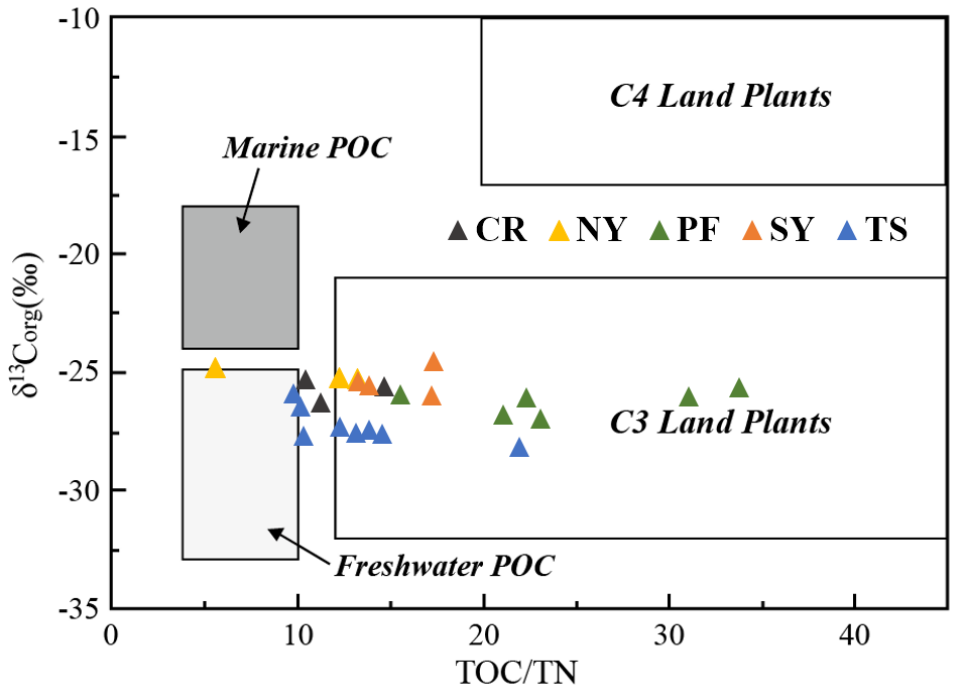

Figure A4 Relationship between $\delta^{13}C$ and TOC/TN ratios of Alaskan samples. Boxes show the fields for different sources of organic matters. Data fields adapted from Lamb et al. (2006).